Article

Marine Heat Waves over Natural and Urban Coastal Environments of South Florida

Yannis S. Androulidakis [1,2,*] **and Vassiliki Kourafalou** [3]

1   Laboratory of Maritime Engineering and Maritime Works, School of Civil Engineering, Aristotle University of Thessaloniki, 54124 Thessaloniki, Greece
2   Laboratory of Physical and Chemical Oceanography, Department of Marine Sciences, University of the Aegean, 81100 Mytilene, Greece
3   Department of Ocean Sciences, Rosenstiel School of Marine, Atmospheric and Earth Science, University of Miami, 4600 Rickenbacker Causeway, Miami, FL 33149, USA
*   Correspondence: iandroul@civil.auth.gr

Abstract: Marine Heat Wave (MHW) events are increasingly recognized as an important factor in the sustainability of coastal environments (both natural and urban), in the context of climate change. They are related to increasing trends of Sea Surface Temperature (SST) at the adjacent ocean waters. SST is an important parameter of the earth's climate and increasing SST trends have been associated with adverse effects on coastal ecosystems, with important environmental and socioeconomic implications. This study focuses on the SST interannual variability over the coastal marine environment of South Florida, which contains several fragile ecosystems, and draws associate effects with adjacent large urban coastal settlements. The methodology is based on high-resolution satellite-derived SST data during a 40-year period (1982–2021), augmented by recent high-resolution model simulations (2012–2020). A generally increasing trend has been detected in the observations over the entire region (0.19 °C/decade). The unusual temperature levels have been associated with the formation of extensive MHW events, which showed interannual positive trends (0.75 events/decade) during the 40-year study period. Specifically, the six most recent years (2015–2021) were characterized by the strongest formation of MHWs with a peak in 2015, 2019 and 2020, with more than 8 events/year and approximately 70 to 110 days/year duration in total. The Florida Keys, especially along the Straits of Florida (southern island coasts), revealed very strong increasing trends. Miami Beach is also characterized by strong interannual trends (1.1 events/decade and 10 days/decade) compared to the enclosed basin of Biscayne Bay. In addition to the influence of atmospheric conditions over all regions around South Florida, the formation of MHWs near the eastern Florida coasts was also controlled by ocean dynamics, related to the warm Florida Current (FC). The evolution of the FC close to the eastern coasts (e.g., Miami Beach) was found to be a pre-condition of MHW formation. Several disastrous events on the biotic environment of South Florida near large urban settlements have been related to the formation of MHWs. The detected positive trends, and especially the recent high peaks of MHW events, may enhance the loss of specific heat-sensitive species, damaging the biodiversity of this tropical coastal environment and weakening the natural coastal protection against tropical storms. Urban planning for sustainable development in South Florida's coastal cities must take into account MHW trends.

Keywords: remote sensing; ocean warming; Straits of Florida; extreme events; climate change

1. Introduction

Marine Heat Wave (MHW) events [1,2] are extreme climatic episodes affiliated with warm Sea Surface Temperature (SST) values that persist for days to months, over a specific oceanic area (the full definition of MHWs is given in Section 2.5). SST is an important parameter of the earth's climate and one of the main indicators of the climate change impacts on the ocean environment [3]. The interannual distribution of the SST and its

increasing trends during the last decades are related both to the variability of the atmospheric conditions and to the ocean circulation dynamics. MHW events may affect the vulnerability of marine organisms and ecosystems [4] and have been observed in all major ocean basins (i.e., [5–12]), especially during the last decade. However, only a few MHWs have been documented and examined in detail [13]. Oliver et al. [14], based on a large range of ocean temperature data (in situ and satellite), showed that the global average of MHW frequency and duration, during the 1925–2016 period, increased by 34% and 17%, respectively. In this study, we assess the interannual and spatial variability of the SST levels over the seas surrounding South Florida, focusing on their effects on the natural and urban coastal environments. We investigate the formation of MHW events during the last 40 years (1982–2021), based on continuous high-resolution satellite-derived data. We also investigate the impact of ocean dynamics, with the aid of high-resolution model simulations and we discuss MHW implications on adjacent natural and urban coastal environments.

We define the study area as the South Florida coastal region (Figure 1) that consists of continental shelves, straits, islands, marine protected areas, and urban settlements. A unique characteristic is the close proximity of a major, warm, deep oceanic current (the Gulf Stream), which manifests itself as the Loop Current/Florida Current system around South Florida. The environmental quality of this region is strongly affected by the temperature levels of the coastal waters. The South Florida coastal region is surrounded by the shallow Western Florida Shelf (WFS) in the west, the Florida Keys and the deeper Straits of Florida in the south, and the narrow Eastern Florida Shelf (EFS) in the east, where the broader Miami metropolitan area with millions of habitants is located. This coastal marine ecosystem comprises mangrove forests, extensive seagrass beds, and the only tropical coral reef tract in the continental United States. Intense human pressures and global climate change factors, such as increased temperature during the last century, pose severe threats on the quality of the South Florida coastal ecosystem [15].
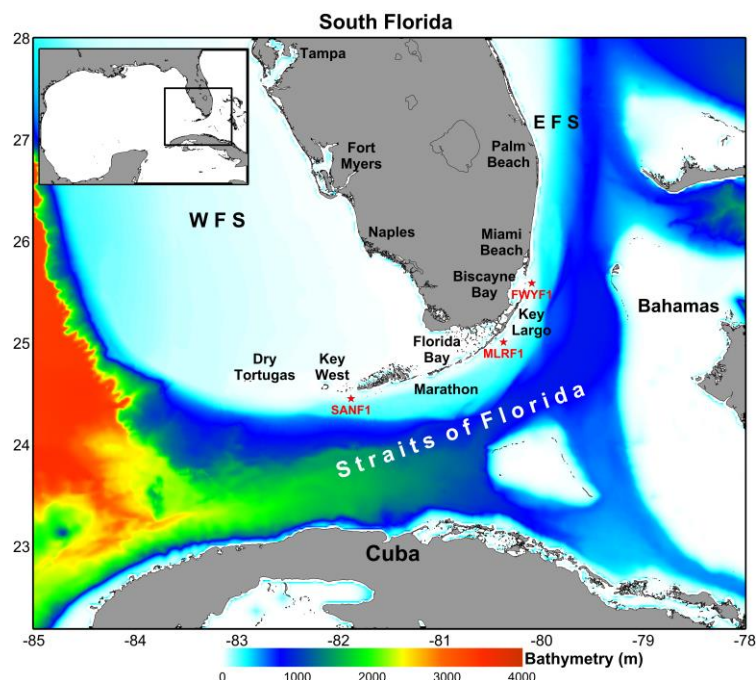

Figure 1. Bathymetry (m) of the South Florida domain with characteristic geographical locations (Western Florida Shelf: WFS and Eastern Florida Shelf: EFS). The locations of the National Data Buoy Center (NDBC) SANF1, MLRF1, and FWYF1 buoys are marked with red stars. The insert map shows the location of the study domain in South Florida.

Kuffner et al. [16], based on long-term in situ measurements, showed evidence of approximately 0.8 °C warming in SST over the Florida Keys during the last century; the

magnitude of warming was similar to the observed global trend. Carlson et al. [17], based on daily 0.25° AVHRR SST data, showed that the August maximum SST in Florida Bay has increased by 1 °C from 1981 to 2016 (~0.030 °C/year) contributing to the seagrass mortality, especially during 1987–1991 and 2015–2016. The SST in the nearshore Atlantic Ocean increased at a rate of 0.023 °C/year. However, Carlson et al. [17] argued that these increasing trends over the WFS and EFS, based on the same low-resolution data (0.25°) and using all months, were very weak and not statistically significant, with large p_{values}, on the basis of the Mann–Kendall [18,19] trend test. Liu et al. [20] presented four main seasonal patterns of SST over the WFS: (a) the winter SST pattern related to the cooling effect of shoaling isobaths on the shelf and the warming influence of advection by the Loop Current, (b) the spring SST pattern that shows a mid-shelf cold tongue, (c) the summer SST pattern characterized by the warming effect of shoaling isobaths on the shelf due to the Loop Current, and d) the autumn SST pattern characterized by a warm tongue on the shelf. Soto et al. [21] showed that years with the highest SST variance (>7 °C) suffered the greatest coral cover lost, while years with intermediate (6–7 °C) and low (<5 °C) SST variances had little or no loss in coral cover. The cold events and their respective cold fronts in the ocean also impact the South Florida coastal waters, with fatal consequences for a large number of corals and associated organisms. Barnes et al. [22], based on an SST climatology derived from satellite data over the 1995–2010 period, showed that the 2010 cold event in January 2010 (https://www.weather.gov/media/mfl/news/2010WxSummary.pdf, accessed on 1 October 2022) was characterized by negative SST anomalies between 11 to 14 °C resulting in extensive benthic mortality [23] and the loss of a large number of cold-sensitive wildlife species [24]. The investigation of the spatial, seasonal and interannual variability of the SST, and the detection of MHW extreme events are crucial to evaluate the quality and resilience of the biotic environment over the entire South Florida coastal region. The study of MHW events requires the understanding of the factors controlling the processes impacting SST.

The SST variability over the South Florida is determined by two main factors: the meteorological forcing (air–sea exchanges and wind stresses), and the respective local and regional ocean dynamics. The latter are mainly controlled by large scale circulation patterns such as the Loop Current along the WFS, continuing as the Florida Current (FC) in the Straits of Florida (southern branch along the Florida Keys and northern branch along the EFS). The Loop Current/Florida Current system around South Florida constitutes the evolution of the Gulf Stream over the region [25], carrying warm Caribbean waters toward the Atlantic Ocean. The meandering of the FC through the Straits of Florida is associated with mesoscale eddy activity to the north (along the Florida Keys; [26]) and the south (along the Cuban coast, [27,28]). The cyclonic eddies [26,29] and the proximity of the FC to the southern WFS [30] affect the local circulation and SST distribution over the southern WFS and the Florida Keys. The Loop Current evolution and the accompanying Loop Current Frontal Eddies [31,32] over the shelf break of the WFS, together with the prevailing atmospheric conditions (winds and heat fluxes), determine the SST variability over the shelf [33–35]. Upwelling and downwelling processes under favorable wind conditions may also alter the surface temperature levels along the western [36,37] and eastern [38,39] Florida coasts. South Florida has a tropical climate, characterized by a wet summer season and a dry one from mid-fall through late spring [40]. Hurricane-induced winds that may occur during tropical storm events (typically from June to November) may control the ocean circulation, the vertical mixing and the SST distribution of the affected coastal regions. The frequency of hurricanes has been rather constant through time, but there is evidence of upward trends in the intensity of the strongest hurricanes, showing increasing trends of the wind speed around 13 ± 6 m/s/century [41].

In this study, we focus on the relationship between MHW events and the spatial and temporal SST variability over the South Florida coastal region during the most recent 40-year period (1982–2021). We have adopted a methodology that uses high-resolution (~5 km) satellite observations, field observations, meteorological data, and numerical hydrodynamic simulations. We discuss the interannual variability and the spatial differences

between coastal regions of South Florida with high environmental interest (e.g., coral reefs, seagrass beds, mangrove forests) or extensive urban infrastructure and population (e.g., Miami metropolitan area). The main motivation of the study is to contribute to the understanding of climate change impacts around the coastal areas of South Florida, by examining the increasing temperature trends (SST) in the surrounding ocean waters and for the first time, the resulting MHWs that can impact the marine and urban environments. The goal is to identify the SST differences between the South Florida sub-regions and the respective coastal waters during the last four decades. This can be potentially useful to the research on the implications between physical and biochemical properties. We will also evaluate the environmental met-ocean factors that are responsible for the interannual SST variability and trends of each coastal area, focusing on the formation of MHWs and their interannual variability over this region. The related along-shore variability and interannual trends along the entire coastal region, which is of great ecological and socioeconomic importance (especially due to coral reef ecosystems, [42,43]), will be also discussed.

More information about the methods and data are given in Section 2. Section 3 presents the main results concerning the SST variability and trends, and the formation of MHWs. Section 4 discusses the atmospheric and ocean effects on temperature distribution. Finally, a summary with concluding remarks is presented in Section 5.

2. Materials and Methods

The data used in the current study consist of satellite observations (SST), atmospheric modeling data, ocean field observations, and simulated ocean fields covering parts or the entire study period (1 January 1982 to 31 December 2021). A summary of the data and their main characteristics is presented in Table 1.

Table 1. Main characteristics of observational and modeling data used in the study (parameter, type, spatial and temporal resolution, area coverage, dataset source).

Parameter	Type	Res.	Step	Period	Area	Source
SST	Satellite	0.05°	Daily	1982–2021	Florida Straits, South Florida, and Florida Keys	Copernicus System
Air temperature (2 m)	ECMWF Reanalysis (ERA5)	0.25°	Hourly	1982–2021	Florida Straits, South Florida, and Florida Keys	Copernicus System
Wind Components (10 m)	ECMWF Reanalysis (ERA5)	0.25°	Hourly	1982–2021	Florida Straits, South Florida, and Florida Keys	Copernicus System
Radiations (Shortwave, Longwave, Sensible, Latent)	ECMWF Reanalysis (ERA5)	0.25°	Hourly	1982–2021	Florida Straits, South Florida, and Florida Keys	Copernicus System
SST	In Situ	Buoy	Hourly	2005 2005–2010 2005–2007	Key West Key Largo Biscayne Bay	NOAA/NDBC
Air Temperature	In Situ	Buoy	Hourly	2012–2020	Biscayne Bay	NOAA/NDBC
Temperature and Currents	Hydrodynamic Modeling	0.01°	6-hourly	2012–2020	Florida Straits, South Florida, and Florida Keys	University of Miami

2.1. Remote Sensing

The dataset of the satellite observations, used in the study, includes Sea Surface Temperature (SST), distributed by the E.U. Copernicus Marine Service (https://www.copernicus.eu/, accessed on 5 August 2022), covering the entire study period from 1982 to 2021 (Table 1). The SST dataset is the Operational SST and Ice Analysis (OSTIA; [44]) global SST reprocessed product at 0.05° horizontal grid resolution, using in situ and satellite data. The satellite-derived data consist of the daily mean gap-free (L4) horizontal fields over the South Florida region (Figure 1). The South Florida SST data were used to analyze the SST

temporal and spatial variability, and to detect the MHWs. Extensive validation of the OSTIA product, based on comparisons with ARGO and drifter data, confirmed the good quality of the SST fields at the global scale (Quality Information Document (https://catalogue.marine.copernicus.eu/documents/QUID/CMEMS-SST-QUID-010-011.pdf, accessed on 1 October 2022). The performance of the product was also tested in the South Florida coastal region with the use of in situ measurements collected by the National Data Buoy Center (NDBC; Section 2.2) and is discussed in Section 3.1.

2.2. Field Observations

Hourly measurements of SST were derived from three NDBC buoys (Figure 1; Table 1), located south of Key West (Buoy SANF1), at a Key Largo coastal region (Buoy MLRF1), and at the entrance of Biscayne Bay (Buoy FWYF1). The field observations of SST were used to evaluate the performance of the satellite-derived SST fields over different periods and coastal areas of South Florida. Air temperature hourly data were also collected at Buoy FWYF1 to evaluate the relation between SST and atmospheric temperature anomalies in Biscayne Bay and Miami Beach.

2.3. Meteorological Data

The meteorological conditions for the study domain and period were derived from the ERA5 hourly data on single levels, distributed by the Copernicus Marine Service (Table 1). The ERA5 dataset is a fifth-generation European Centre for Medium-Range Weather Forecasts (ECMWF) reanalysis that combines model data with observations (data assimilation), providing hourly estimates for a large number of atmospheric quantities. Herein, we used the meridional and zonal components of the wind at a height of 10 m above the sea surface to estimate the variability of the wind speed over the ocean waters of South Florida (land values excluded) during the 1982–2021 period. In addition, we also used the air temperature at 2 m above the surface, which is produced by the interpolation between the lowest model level and the Earth's surface, taking into account the atmospheric conditions. The hourly surface net shortwave solar radiation (Q_S), the surface net longave backcatter radiation (Q_b), the surface sensible heat flux (Q_h), and the surface latent heat flux (Q_e) were also collected by the ERA5 dataset to estimate the interannual variability of the surface net heat flux (Q_T; Equation (1)) over the 1982–2021 period.

$$Q_T = Q_S + Q_b + Q_e + Q_h \tag{1}$$

where Q_S and Q_b represent the radiative terms, while the Q_h and Q_e represent the turbulent terms. The ERA5 radiation fields are suitable to evaluate the long-term interannual variability of the heat fluxes over regional basins [45]. The spatial resolution of the atmospheric hourly fields is 0.25°.

2.4. Hydrodynamic Simulations

The hydrodynamic simulations are based on the Florida Straits, South Florida, and Florida Keys Hybrid Coordinate Ocean Model (FKEYS-HYCOM; Kourafalou and Kang, 2012) and cover a 9-year period (2012–2020). HYCOM (http://hycom.org, accessed on 10 October 2022; [46–48]) is a state-of-the-art, three-dimensional hydrodynamic model with advanced mixing schemes and employs a flexible (hybrid) vertical coordinate system (isopycnal, Cartesian, and sigma discretizations) that is advantageous for the topographically complex study area (Figure 1). FKEYS-HYCOM employs 26 hybrid vertical layers and significantly high horizontal resolution of 1/100°, or 900 m as compared to 1/25°, 3.6 km in the GoM-HYCOM outer model that provides the boundary conditions [49]. The model domain covers the area from 78.08° W to 84.528° W and 22.188° N to 27.58° N (Figure 1). The topography was derived from a high-resolution (1/100°) regional Gulf of Mexico bathymetry developed at the Florida State University/COAPS with a minimum depth of 1 m. The FKEYS-HYCOM vertical coordinates are maintained in isopycnic mode in the "open sea" domain (e.g., Straits of Florida), they smoothly transform to bottom following

(sigma) and/or Cartesian (fixed z-level) coordinates in the mixed layer, and in the coastal and shelf areas (e.g., Florida shelves, northern Cuban coast and shallow banks). Atmospheric forcing is provided by the Navy Global Environmental Model (NAVGEM, [50]). The FKEYS-HYCOM has been validated with satellite [26,27] and in situ [51] data, showing additional skill in reproducing the circulation patterns and capturing the FC evolution in the Straits of Florida. We used the model outputs to derive the FC location in the Straits of Florida and evaluate its impact on the coastal SST variability.

2.5. Detection of Marine Heat Waves

The study adopts the definition proposed by Hobday et al. [1] to determine the MHW events, based on abrupt SST increases above a "climatologic" value (the baseline temperature) for a certain time period. This approach has been broadly used to evaluate the MHW variability in both global ocean (i.e., [14,52]) and regional basins (i.e., [9,10,12,44,53]). To define a baseline temperature, Hobday et al. [1] proposed a period of 30 years, which is associated with the time scale variability of ocean drives (e.g., El Nino). Herein, we use a longer dataset of 40 years with satellite-derived SST fields (see Section 2.1). According to this definition, a MHW is defined as a discrete and prolonged anomalously warm ocean-based event. Hobday et al. [1] also pointed out that a MHW should be defined relative to a baseline period and a particular time of the year from which the intensity, duration and spatial extent of the MHW could be defined. This also means that a MHW is not just limited to the warmer months, since for some biological applications the consideration of heatwaves in colder months is essential. The term 'discrete' implies that the MHW is an identifiable event with clear start and end dates; 'prolonged' means that it has a duration of at least 5 days. Gaps, between events of two days or less with subsequent five days or more, will be considered as a continuous event. 'Anomalously warm' means that the water temperature is warm compared to the baseline temperature. The baseline temperature used in the present study is defined by the seasonal (monthly) varying 90th percentile, derived from the 1982–2021 SST data in the resolution ($0.05°$) of the South Florida domain. Moreover, the duration (the time between the start and end dates; ≥ 5 days) was also computed for all detected MHW events. The intensity of the MHWs was examined based on the methodology introduced by Hobday et al. [2]. The goal is to set categories of MHWs on multiples of the value represented by the local difference between the climatological mean and the 90th percentile baseline, which is the threshold used to identify MHWs. Multiples of this local difference will describe different categories of MHWs. Magnitude of scale descriptors, defined as moderate (1–2× times, Category 1), strong (2–3× times, Category 2), and severe (>3× times, Category 3), can be allocated at each point in space and time of an MHW event.

3. Results

3.1. Evaluation of Satellite-Derived SST at Coastal Areas

The quality of the SST fields at coastal areas is tested, based on the comparison with in situ temperature measurements (Figure 2) collected at three locations (NDBC buoys) along the Florida Keys and Biscayne Bay (Figure 1). The NDBC SST in Fowey Rock, at the vicinity of Biscayne Bay (Buoy FWYF1), followed a clear seasonal variation from January 2005 to May 2007 (Figure 2a) with a mean level of 26.6 °C (Figure 2b). The satellite-derived timeseries followed a similar distribution revealing a very high correlation (R_p: Pearson Correlation Coefficient) and a small Root Mean Square Error (RMSE) with the field measurements ($R_p = 0.97$ and RMSE = 0.68 °C; Figure 2b); the respective mean value (26.42 °C) is slightly smaller than the one measured directly at the sea surface. The agreement between the two products is better at Buoy MLRF1, located at the Key Largo coastal area (Figure 1), where both timeseries showed a similar increasing trend (Figure 2c) and a linear regression very close to the x = y identity line (Figure 2d). The Pearson correlation coefficient and the RMSE confirm the very good performance of the satellite-derived data ($R_p = 0.98$ and RMSE = 0.50 °C; Figure 2d). The correlation is even higher at the

lower Keys (Buoy SANF1; Figure 1) during 2005, when the Pearson coefficient is $R_p = 0.99$ and the RMSE is less than 0.5 °C (Figure 2f). The satellite-derived SST data are capable to describe all short-term peaks and lows that exceed the typical range of the seasonal cycle; the extremely high values in August 2005 (>31 °C) and the large drop of approximately 2 °C at the end of the same month (28 °C) are apparent at both field and satellite timeseries (Figure 2e). Thus, we conclude that the high-resolution satellite-derived SST daily fields are suitable to investigate not only the open sea and shelf SST variability [44] but also the temperature distribution and the formation of MHWs over the South Florida coastal region.
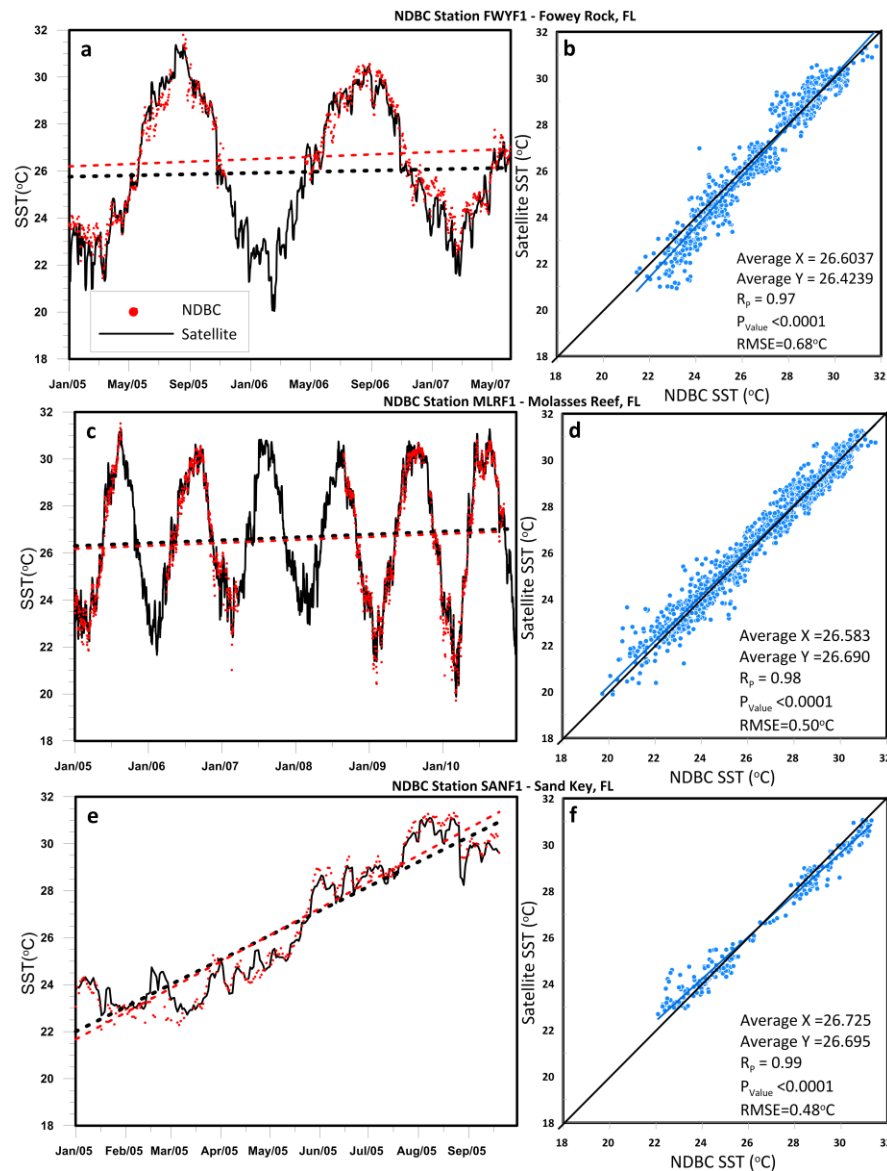

Figure 2. (**a**) Daily evolution of Sea Surface Temperature (SST; °C) derived from the satellite data (black line) and the NDBC Stations (red dots) (**a**) FWYF1 (coastal area of Miami), (**c**) MLRF1 (Upper-Keys), and (**e**) SANF1 (Lower-Keys). The respective scatter diagrams (**b**,**d**,**f**) between the two timeseries for each case are also shown. The linear regressions (trends and timeseries comparison), the mean values, the Pearson correlation coefficients (R_p), the tests of statistically significant correlation (p_{value}), and the Root Mean Square Errors (RMSEs) for all cases are presented.

3.2. Interannual Variability of SST

The mean annual SST levels over the entire study domain revealed an increasing trend during the 1981–2021 period, following the respective air temperature interannual

trend (Figure 3a). In addition to the Mann–Kendall method that identifies the trend, we employ the Sen's slope [54] to characterize the magnitude of the change. We found that both trends are characterized by positive Sen's Slopes of 0.19 °C/decade and coefficient of determination R^2 = 0.46 for SST, and 0.21 °C/decade and R^2 = 0.42 for air temperature. The increasing trends are statistically significant (p_{value} < 0.01: statistical significance level 99%). The SST values ranged around 26.3 °C in 1982 and reached the mean level of 27 °C 40 years later, in 2021. The highest peaks were observed after 2015 and especially during 2019–2020, when the mean annual SST over the entire region reached the level of 27.4 °C. On the contrary, the lowest annual level was observed in 1984 (<26 °C). Despite the general positive trend, a period of relatively low SST that flattened the linear trend occurred between 2004 and 2013, following a similar stagnation period in the air temperature levels, which revealed a significant drop in 2010 (<24 °C). A respective increasing trend was also computed for the 99th SST percentiles, that represent the highest values of each year (Figure 3b). The 99th percentile of SST revealed a steeper trend over the 40-year period characterized by a higher statistical significance (p_{value} < 0.01) Sen's Slope (0.21 °C/decade; R^2 = 0.35) in comparison to the mean values. The beginning and the end of the period show a mean difference of approximately 1.5 °C. The highest and lowest 99th percentiles of SST were also computed for 2019 and 1984, respectively. The increasing trend that was computed for the minimum SST levels was milder than the mean and maximum values, while the positive Sen's Slope was smaller (0.05 °C/decade) and not statistically significant (p_{value} > 0.01). A year of very distinctive behavior was 2010, when although the colder air conditions prevailed (<24 °C; Figure 3a) and the lowest minimum SST levels also occurred (Figure 3c), the 99th percentile was relatively high (30.7°; Figure 3b) resulting in the largest annual variance among all years (>9 °C; Figure 3d). According to Soto et al. (2011) findings, 2010 can be characterized as a year of high risk on coral losses. The cold January of 2010 (Colella et al., 2012) affected the water temperature levels and reduced the mean annual levels, but very high SST levels also occurred during the summer period, increasing the 99th percentile annual variance. It is concluded that the observed general increasing trend is mainly related to the summer maximum values and less related to increases during the winter periods. For most of the years, the variance of the annual values ranges between 5 °C and 6 °C, with a very small increasing trend throughout the entire period (0.05 °C/decade; Figure 3d). Even though the variance showed a small increasing trend, indicating larger seasonal differences, the annual variance is relatively small (<5 °C) during the last decade (2012–2021), when all winter and summer levels were high, confirming the general warming of the ocean; the highest minimum temperatures were observed during the same period (Figure 3c).

3.3. Spatial Variability of SST

The spatial variability of the seasonal 10th and 90th percentiles is presented in Figure 4. The 10th percentile represents the 10% chance that the temperature fell below this threshold during the study period; anything below the 10th percentile is considered unseasonably cool. Very low temperature levels, associated with cold water events, may have fatal consequences on coral communities [22] but may also reduce the occurrence frequency of the MHW events during the winter months [12]. The 90th percentile describes the 10% chance that SST was above this threshold, and anything above it is considered unseasonably warm. The monthly 90th percentile was used as the temperature climatology (threshold) for the MHW computation (see Section 3.4). The colder waters have been detected over the entire WFS between January and March (<17 °C; Figure 4), while very low SST also occurred along the western Florida coast in December. Over the same areas and months, the 90th percentiles were relatively low (<24 °C) revealing their lowest values between the coastal region of Tampa (28° N) and Fort Myers (26° N). The highest 10th and 90th percentile values were computed during July-September for the entire study domain; especially the 10th percentiles were homogenously distributed over all areas. The maximum 90th percentiles were computed over the southern WFS (>31 °C), and especially along the northern coasts

of the Florida Keys during the summer months and early fall. The high 90th percentiles are an indicator that the detected MHWs over these areas are characterized by unusual high SST levels (see Section 3.4). The open waters of the Straits of Florida were characterized by high 90th percentiles during winter and spring but lower levels than the WFS and EFS areas during the summer months, due to the FC evolution that controls the distribution of physical properties over the Straits (see Section 4.2). Two distinctive seasonal changes are detected during the annual cycle: one during June, when both 10th and 90th percentiles revealed a strong increase over the entire study domain, and a second in November, when both metrics showed significant reductions.
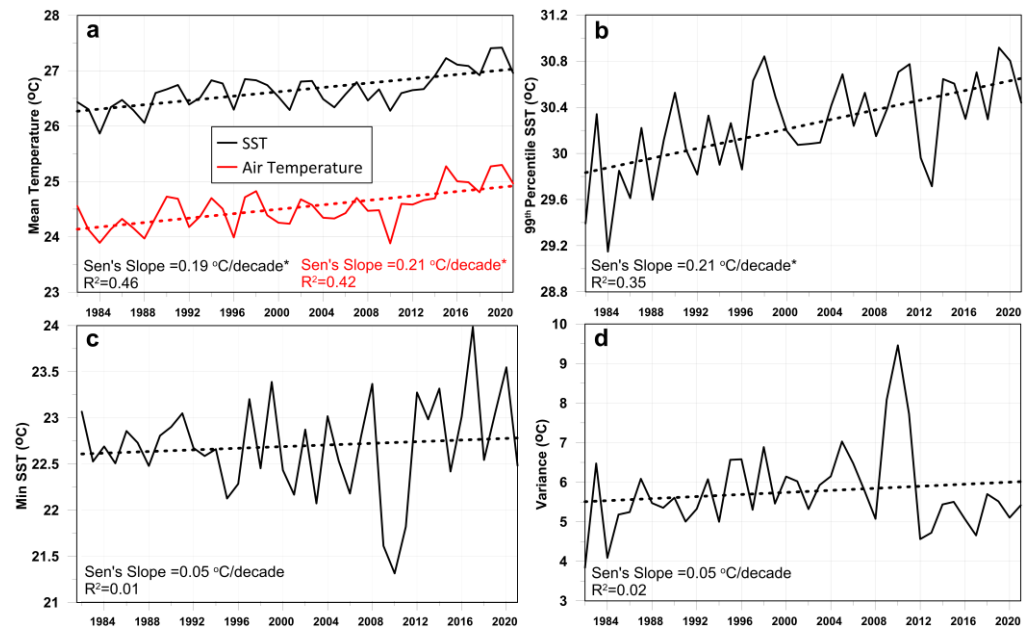

Figure 3. Annual variability (continuous lines) and trends (dashed lines) of: (**a**) the mean sea surface temperature (SST; °C) and air temperature (Air Temp; °C); (**b**) the 99th percentile of SST; (**c**) the minimum (min) SST; and (**d**) the variance, averaged over the entire study domain (Figure 1) for the period 1982–2021. The Sen's Slope and coefficient of determination (R^2) for each trend are presented. The asterisk (*) indicates that the hypothesis that the trend is statistically significant is true (99% MK test of statistically significant trend: $p_{value} < 0.01$).

We focus on the coastal, island and shelf (WFS and EFS; <300 m) areas over the South Florida region and estimate the spatial variability of the interannual trends and maximum levels of the SST (Figure 5). The warmest coastal areas (>26 °C) were detected over the EFS (south of West Palm Beach), south of the Florida Keys and over the southwestern WFS (Figure 5a). The broader Tampa area in the West and coasts north of the West Palm Beach in the East showed the lowest mean values (<24.5 °C), while relatively low levels (~25 °C) were also detected in the West between Fort Myers and Naples. The highest 99th percentiles that represent the maximum SST levels, were computed for the entire southwestern Florida coast, the Florida Keys, and the Biscayne Bay (>31 °C; Figure 5b); values over 32.5° were observed in Florida Bay, inside the bay of Fort Myers and north of the Florida Keys. The broader WFS, the Dry Tortugas, the area south of the Florida Keys and the EFS showed 99th percentiles around 30.7 °C, while the lowest maximum levels occurred north of West Palm Beach (<30 °C). The general trend of the mean SST for the broader region was 0.19 °C/decade (Figure 3) mainly over the western WFS and in the coastal region south of the Florida Keys (Figure 5c), where it was statistically significant (99%; Figure 5d). The coastal areas of western Florida, the northern Florida Keys, and the northern EFS revealed the lowest Sen's Slopes (<0.14 °C/decade; Figure 5c); the areas north of West Palm Beach, Naples, south of Fort Myers, and Tampa also showed p_{values} higher than 5% indicating the weak statistical significance of the trends based on the

95% MK trend test (Figure 5d). The other coastal regions that exhibited weak trends, although they revealed small Sen's Slopes, had p_{values} lower than 5% (areas inside the 95% contour; red line in Figure 5d), confirming the statistical significance of the respective trends. Biscayne Bay showed Sen's Slopes around 0.11 °C/decade, while the trend of the ocean side of Miami Beach was stronger (0.14 °C/decade) and more statistically significant ($p_{value} < 0.01$). Stronger trends were computed in Florida Bay (>0.17 °C/decade), although the trend was milder (<0.13 °C/decade) at the rest of the southern WFS (north of Florida Keys). North of Key West, the computed weak trends were also associated with very high p_{values}, indicating negligible interannual trend over the 1982–2021 period. The spatial variability of the SST trends is also projected in the distribution of the MHW occurrence frequencies and interannual trends (see Section 3.4).
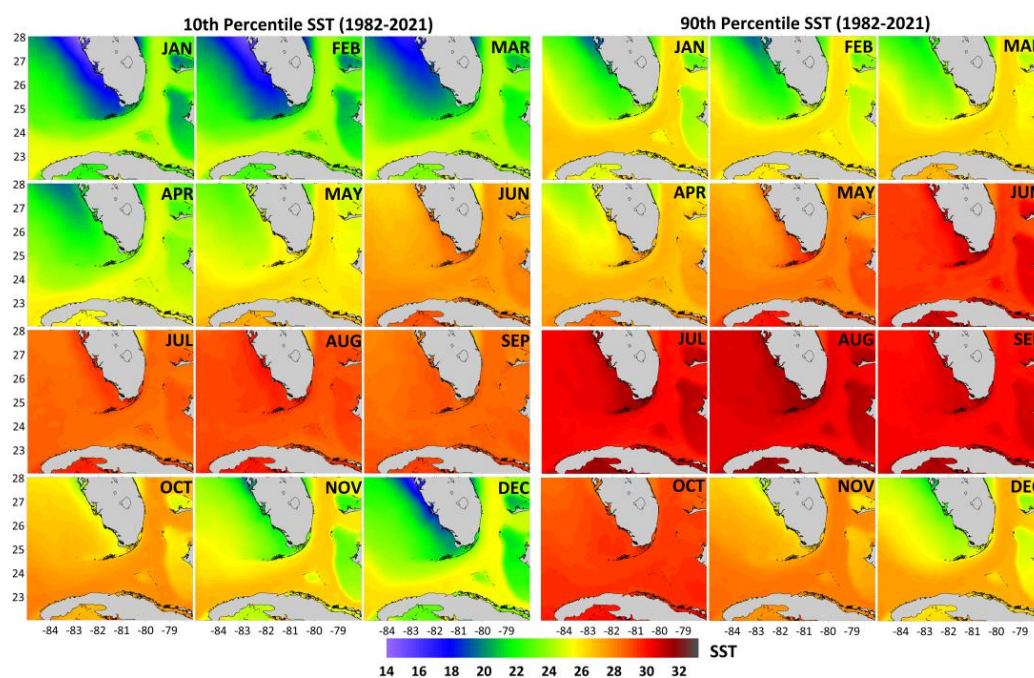

Figure 4. Horizontal distribution of the monthly 10th (**left panels**) and 90th (**right panels**) percentiles of SST derived from the daily satellite data over the 1982–2021 period. The monthly horizontal levels of 90th percentiles represent the monthly climatological baseline of the Marine Heat Wave (MHW) estimation.

3.4. Formation of Marine Heat Waves

3.4.1. Spatial Variability and General Trends

The formation of MHWs was computed and analyzed for the entire study region, and for the whole time period. Both the annual number of MHW events and their total annual durations (days), which were averaged over the South Florida domain, revealed an increasing trend during the 40-year period and are statistically significant ($p_{value} < 0.01$; Figure 6a). The increase of the total annual MHW days was 7.4 days/decade, and the respective increase of the MHW events was 0.75 events/decade. Three large peaks were computed in 2015, 2019, and 2020, respectively, with more than 8 MHWs lasting around 70 to 110 days in total, constituting the high peaks of the mean SST values presented in Figure 3a. The prolonged period of low SST levels reported during the 2004–2013 decade (Figure 3a) agrees with the low number of MHWs events (<4) and days (<40) (Figure 6a). However, the period with the lowest SST levels in 2010 does not coincide with the lowest MHW events since the reduced SST were mainly associated with the very cold waters of the winter months. The last seven years (2015–2021) revealed the highest number of events and durations among all study years, with the exception of 2018, when very few (4) and short (<40) MHWs that were observed in the South Florida region.
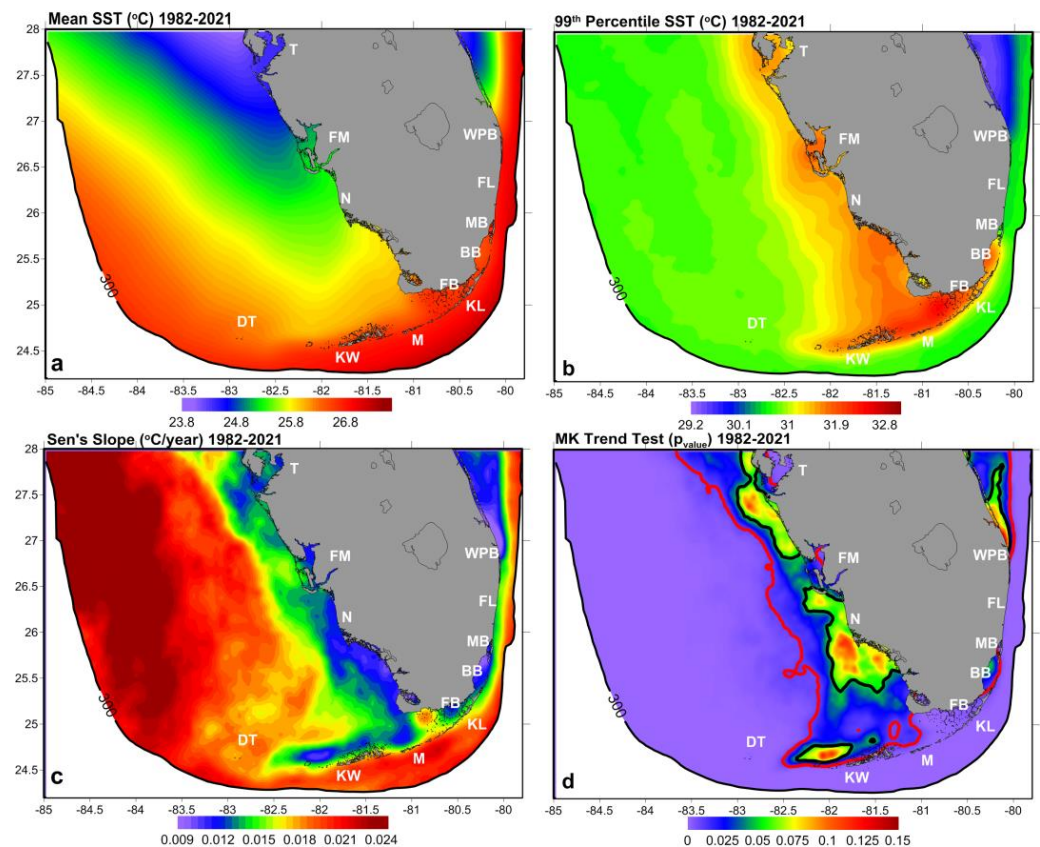
Figure 5. Horizontal distribution of (**a**) Mean Sea Surface Temperature (SST; °C), (**b**) 99th Percentile SST (°C), (**c**) Sen's Slope (°C/year) and (**d**) p_{value} of the MK test of statistically significant trend, derived from the mean annual values (40 years; red and black contour lines indicate the 99% and 95% thresholds, respectively), derived from the daily values of the 1982–2021 period over the South Florida shelf areas (less than 300 m depth). The black solid lines at the periphery of all plots indicate the 300 m isobath around South Florida. The main coastal and urban sites are also marked, similar to Figure 1 and abbreviated here (clockwise from top right, WPM: West Palm Beach; FL: Fort Lauderdale; MB: Miami Beach; BB: Biscayne Bay; FC: Florida City; KL: Key Largo; M: Marathon; KW: Key West; DT: Dry Tortugas; N: Naples; FM: Fort Myers; T: Tampa).

We followed the methodology introduced by Hobday et al. [2] to base categories of MHWs (see Section 2.5). The vast majority of the events detected over the South Florida domain are characterized as moderate (Figure 6b), revealing an almost identical interannual distribution of number and duration as all MHWs together (Figure 6a). The Sen's Slopes of the number and duration are 0.73 events/decade and 6.7 days/decade, respectively; both are statistically significant. The Category 2 MHWs (strong events; Figure 6c) also revealed statistically significant increasing trends, with lower though gradients (0.01 events/decade and 0.5 days/decade) than Category 1 events. Two peaks of strong MHWs were observed in 2003 and 2020, when the highest SST levels were measured (Figure 3a). A small number of strong events, but with extended duration, were also observed in 2017. On the contrary, in 1984, MHWs were not formed at all over the entire region. Severe events (Category 3) occurred only after 2003, but with limited occurrence, while MHWs were observed every year only during the last seven years (after 2015), resulting in very weak interannual trends which are not statistically significant over the 40-year study period. However, severe MHWs occurred in the summer of 2010, in agreement with the high 99th percentiles (Figure 3b), although very low minimum SST values occurred during that winter (Figure 3c) in agreement with the large SST variance of that year (Figure 3d).
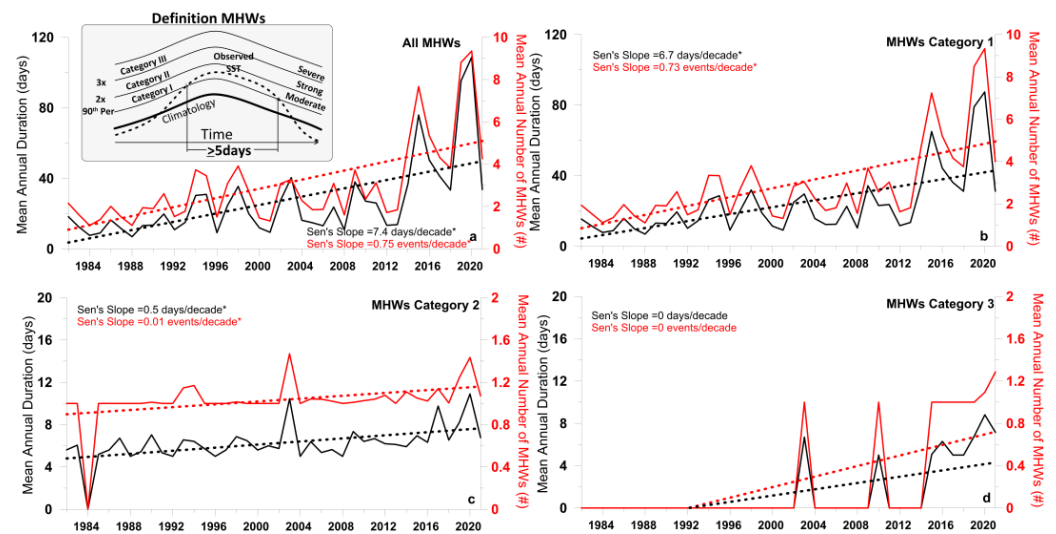
Figure 6. (**a**) Interannual evolution of the mean annual number of all Marine Heat Waves (MHWs; red line) and the mean annual duration (days; black line) derived from all satellite daily data at each satellite grid point of the study area for the 1982–2021 period; the insert panel presents the categorization schematic for MHWs showing the observed temperature timeseries (dashed line), the long-term regional climatology (bold line), and the 90th percentile climatology (thin line). Multiples of the 90th percentile difference (2× twice, 3× three times) from the mean climatology value define each of the Categories 1–3, with corresponding descriptors from moderate to severe [2]. The individual evolution of the mean annual number and duration of MHWs for Category 1, 2, and 3 are presented in (**b**–**d**), respectively. The zero MHW cases were not included in the calculations. The linear trend (dashed line), the Sen's Slope, and the respective test of statistically significant trend (p_{value}) for each case are presented. The asterisk (*) indicates that the hypothesis that the trend is statistically significant is true (99% MK trend test: $p_{value} < 0.01$).

The spatial distribution of the mean annual and total number of MHWs over the entire study domain is presented in Figure 7. The highest mean annual number of events was computed over the southern WFS, along the northern coasts of the Florida Keys and inside the Florida Bay showing approximately 3 events per/year (Figure 7a) and more than 110 events during the 40-year period (Figure 7c). Although fewer events usually formed over the northern parts of the WFS (2–2.5 events/year and less than 100 in total for 40 years), their duration was longer and therefore the total annual duration over the shelf was homogenously distributed between 24 to 30 days/year (Figure 7b) and more than 1000 days over the 1982–2021 period (Figure 7d). The Straits of Florida, where the warmer waters of the FC prevail, are characterized by fewer events with smaller durations due to the constant high 90th percentile levels that were used as thresholds in the MHW detection. However, the meandering of the FC and its approach toward the Florida coasts plays an important role on both local circulation over the coastal region and the distribution of the physical properties (see Section 4.2). The coastal region of the Bahamas can also be considered as a "hot spot" for MHWs with high number of events (>100; Figure 7c) and long durations (>1000 days; Figure 7d) during the 1982–2021 period.

3.4.2. Variability of MHWs at Coastal and Urban Areas

Ten coastal areas of South Florida with urban and environmental interest (insert maps in Figure 8) were chosen to further analyze the formation and variability of MHW events during the 1982–2021 period. The mean annual number and duration of events, and the mean annual SST for each coastal area are presented in Figure 8. The respective Sen's Slopes of all 40-year trends and their statistical significance tests (p_{values}) are presented in Table 2. The broader Miami coastal area is investigated focusing on two sub-regions: the enclosed basin of Biscayne Bay (Figure 8c), which is relatively protected from ocean influence, and

Miami Beach (Figure 8b), which is more exposed to offshore dynamics of the northern Straits of Florida. Although Biscayne Bay showed a larger number of events over the entire study period (Figure 7c), the increasing trend of Miami Beach is steeper (1.1 events/decade; Table 2), resulting in the formation of more events, especially during the last seven years (Figure 8b). Respectively, the Sen's Slope of the duration is 10 days/decade for Miami Beach and 7.2 days/decade for Biscayne Bay. Biscayne Bay also showed a smaller SST trend (0.1 °C/decade), in agreement with the spatial distribution of trends presented in Figure 5c, compared to the Miami Beach trends (0.15 °C/decade; Table 2). All trends are statistically significant but the Biscayne Bay p_{values} were higher (Table 2; Figure 5d), especially for the SST trend ($p_{value} = 0.021 > 0.01$), thus featuring an overall less significant trend. In 2019 and 2020, more than 9 events occurred in the coastal area of Miami Beach with 100 days total duration (Figure 8b), while less than 8 events with total duration around 75 days occurred in Biscayne Bay (Figure 8c). Biscayne Bay had shown more frequent MHWs until 2010 in comparison to Miami Beach, where several years without any formations were detected during the same period (e.g., 1983–1985, 1988, 1996, 2001, 2008; Figure 8b). Miami Beach is actually characterized by stronger interannual variations, showing years with both larger and smaller number of events, in comparison to the enclosed Biscayne Bay. The offshore ocean dynamics that contribute to this variability are discussed in Section 4.2.
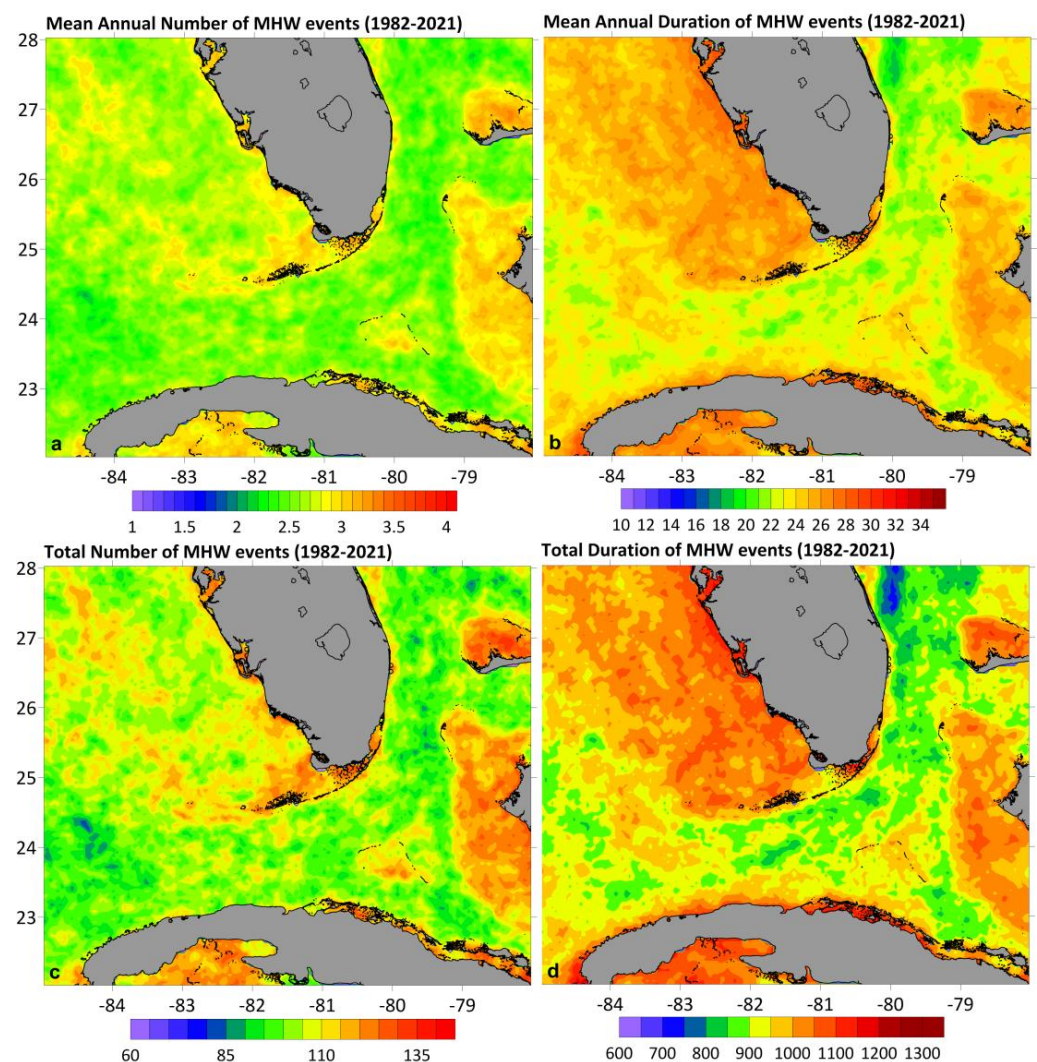

Figure 7. (**a**) Mean annual number, (**b**) mean annual duration (days), (**c**) total number, and (**d**) total duration (days) of MHW events derived from the satellite observations of the 1982–2021 period.
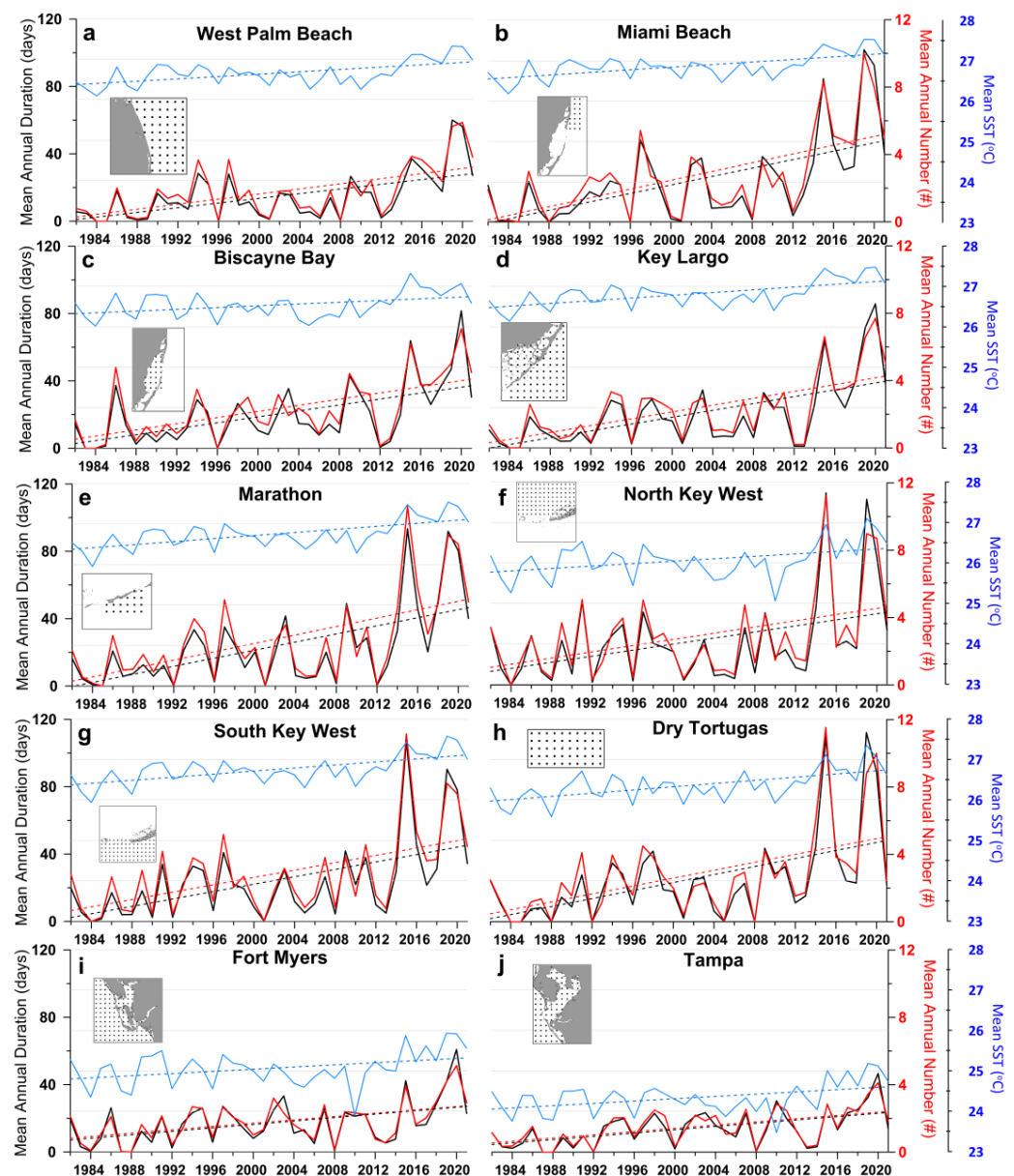
Figure 8. Interannual variability of annual mean number (red solid line), duration (days; black solid line) of MHW events, the mean annual SST (°C; blue solid line) over (**a**) West Palm Beach, (**b**) Miami Beach, (**c**) Biscayne Bay, (**d**) Key Largo, (**e**) Marathon, (**f**) North Key West, (**g**) South Key West, (**h**) Dry Tortugas, (**i**) Fort Myers, and (**j**) Tampa from 1982 to 2021. The insert maps show the satellite grid points used for the computation over each area. The respective linear trends are also indicated with dashed lines.

The northern area of West Palm Beach showed weaker trends (Table 2; Figure 8a) of the MHWs number (0.7 events/decade) and duration (5.6 days/decade). The largest number of events was detected in 2019 and 2020 (>6; Figure 8a) when the highest mean annual SST was also occurred (27.5 °C). Generally, the total annual duration ranged below 40 days throughout the entire study period. The broader area of the northern EFS, where West Palm Beach is located, showed very low 99th percentiles of SST (Figure 5b) with statistically insignificant SST trends (Figure 5c,d). Even weaker trends were computed for Tampa (0.5 events/decade, 4.9 days/decade and 0.12 °C/decade) and Fort Myers (0.5 events/decade, 4.6 days/decade and 0.14 °C/decade), located at the coastal area of WFS (Table 2). Especially in Fort Myers, the p_{values} were the highest among all coastal areas, showing statistically insignificant trend for the mean SST, based on the 99% MK trend

test (p_{value} = 0.045). The lowest number of events with small durations were observed at Tampa, where the highest mean annual number of MHWs, averaged over the Tampa coastal area grid points, was slightly over 4 events in 2020. These small MHW levels and weak trends are mainly related to the domination of colder waters detected from December to March and the very low SST that were measured along the western Florida coast, where the 90th percentiles revealed their lowest values between the coastal region of Tampa and Fort Myers (Figure 4).

Table 2. Sen's Slope (days/decade and events/decade) and p_{values} (test of statistically significant trend) derived from the MK trend test representing the statistical significance of each trend for the Mean Annual Duration and the Mean Annual Number of Marine Heat Wave (MHW) events, and the Mean Annual Sea Surface Temperature (SST) for the 10 coastal areas presented in Figure 8.

Coastal Area	Mean Annual Duration		Mean Annual Number MHW		Mean Annual SST	
	Sen's Slope	P_{value}	Sen's Slope	P_{value}	Sen's Slope	P_{value}
West Palm Beach	5.6	0.0005	0.7	0.0002	0.14	0.001
Miami Beach	10	<0.0001	1.1	0.0001	0.15	0.0005
Biscayne Bay	7.2	0.0002	0.9	<0.0001	0.1	0.021
Key Largo	7.9	0.0002	0.9	<0.0001	0.16	0.0002
Marathon	9.3	0.0007	1.0	0.0007	0.18	0.0002
North Key West	4.6	0.0486	0.6	0.022	0.14	0.036
South Key West	7.5	0.0007	0.8	0.0008	0.18	<0.0001
Dry Tortugas	7.6	0.0011	0.8	0.0011	0.18	<0.0001
Fort Myers	4.6	0.0088	0.5	0.0053	0.14	0.045
Tampa	4.9	0.0006	0.5	0.0003	0.12	0.021

Different trends were computed between the north and south coastal areas of the Florida Keys. Although the northern coasts of the Florida Keys (southern WFS) summed more events during the entire study period (Figure 7c), showing larger annual numbers of MHWs especially before 2008, the general Sen's Slopes are weaker in the North Key West (Figure 8f) than in the South Key West area (Figure 8g) for all variables (number of events, duration and mean SST; Table 2). The broader area of Dry Tortugas showed significantly high interannual slopes (Figure 8h) with more than 11 events lasting approximately 110 days in 2015; very high numbers were also computed for 2019 and 2020. The southern coastal area of Marathon (Figure 8e) was also characterized by high Sen's Slope of MHW events (1.0 event/decade) and the strongest interannual trend of the event durations among all areas (9.3 days/decade). Very strong trends were also computed for Key Largo (0.9 events/decade, 7.9 days/decade and 0.16 °C/decade). The coastal areas of the Dry Tortugas and Florida Keys, and especially along the Straits of Florida (southern coasts), are characterized by very strong increasing trends with high frequencies of MHW events, especially during the last seven years (2015–2021; Figure 8). The highest number of events over the Florida Keys before 2015 were computed for 1997 and 1998 (Figure 8) during the El Niño event, causing extensive coral bleaching ([55]; see Section 4.3). The increasing numbers of MHWs along the southern coastline of the Florida Keys during the last decade agree with the stronger and statistically significant trends of SST computed over the same areas (Figure 5).

4. Discussion

4.1. Effects of Atmospheric Conditions on SST Variability

The air temperature variability averaged annually and over the entire study domain is presented in Figure 3a, showing a similar but slightly sharper interannual trend than the SST increase during the 40-year period. The air temperature and the the respective net heat flux variability are both well correlated with the formation of MHWs showing all significant increasing trends (Figure 9). The highest mean annual air temperatures and the strong positive (downward) heat fluxes generally coincide with the MHW peaks. The Sen's Slope of all trends are statistically significant (p_{value} < 0.0001), with lower significance for the heat fluxes (p_{value} = 0.0142), which also show smaller correlation with the MHW frequency (R_P = 0.44) in comparison to the air temperature (R_P = 0.84).
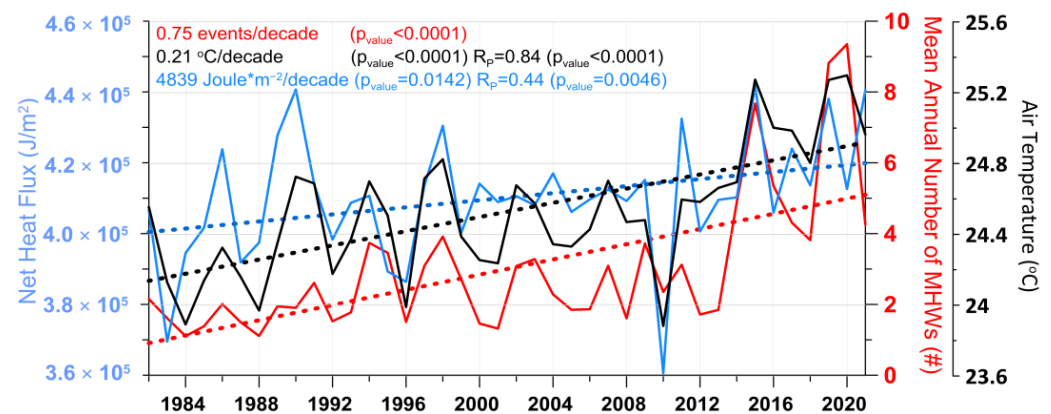

Figure 9. Annual variability (continuous lines) and trends (dashed lines) of the mean annual number of all Marine Heat Waves (MHWs; red line), the air temperature (°C; black line), and the surface net heat flux (J/m^2; blue line). The Sen's Slopes and the Pearson correlation coefficients between both atmospheric variables (air temperature and heat flux) and the number of MHWs are presented. The p_{values} of the MK trend and correlation tests are also shown.

The correlation coefficients between the SST and air temperature timeseries show a strong spatial variability over the South Florida region (Figure 10a). High correlations were computed over the inner WFS with very large correlation coefficients (>0.90) at the broader Tampa and Fort Myers bays, confirming the determining role of air temperature on the SST variability over the western Florida coastal zone; the inner parts of these two bays revealed the weakest impact of air temperature on SST (smaller correlation coefficients). The impact of air temperature on SST gradually reduces towards the WFS shelf slope (0.85–0.75), an area where the Gulf of Mexico mesoscale ocean circulation patterns usually prevail [34]. Loop Current interactions with the WFS shelf control the physical characteristics over the slope contributing to the upwelling of colder waters toward the surface layers [30] or supply warmer Loop Current waters over the shelf through advection [56]. Very strong correlation was also detected at the Bahamas area, which was characterized as a "hot spot" for the formation of MHWs (Figure 7). Relatively low correlation coefficients were computed over the Straits of Florida, and especially west of 83° W and east of 81° W, with very weak correlation along the northern Straits and the EFS (R_p < 0.80). The lower values mainly occurred over the area where the FC flows, controlling the distribution of physical properties (see Section 4.2). The lowest correlation coefficients (R_p < 0.75) were computed at the coastal area north of Miami Beach (26° N). The lag (in days) between the two parameters is around 5 days (R_p = 0.90; Figure 10c). Once the seasonal cycle is removed, the interaction between them is more direct, showing smaller correlation (R_p = 0.57) with a 3-day lag (Figure 10e). The agreement between the two parameters confirms that the effect of the atmospheric temperature on the ocean sea surface temporal and spatial evolutions also holds for the nearshore and coastal study areas. This effect varies among different marine

regions because of other environmental factors, both atmospheric (e.g., wind speed) and oceanic (e.g., river plumes, lateral fluxes, vertical mixing, general circulation).
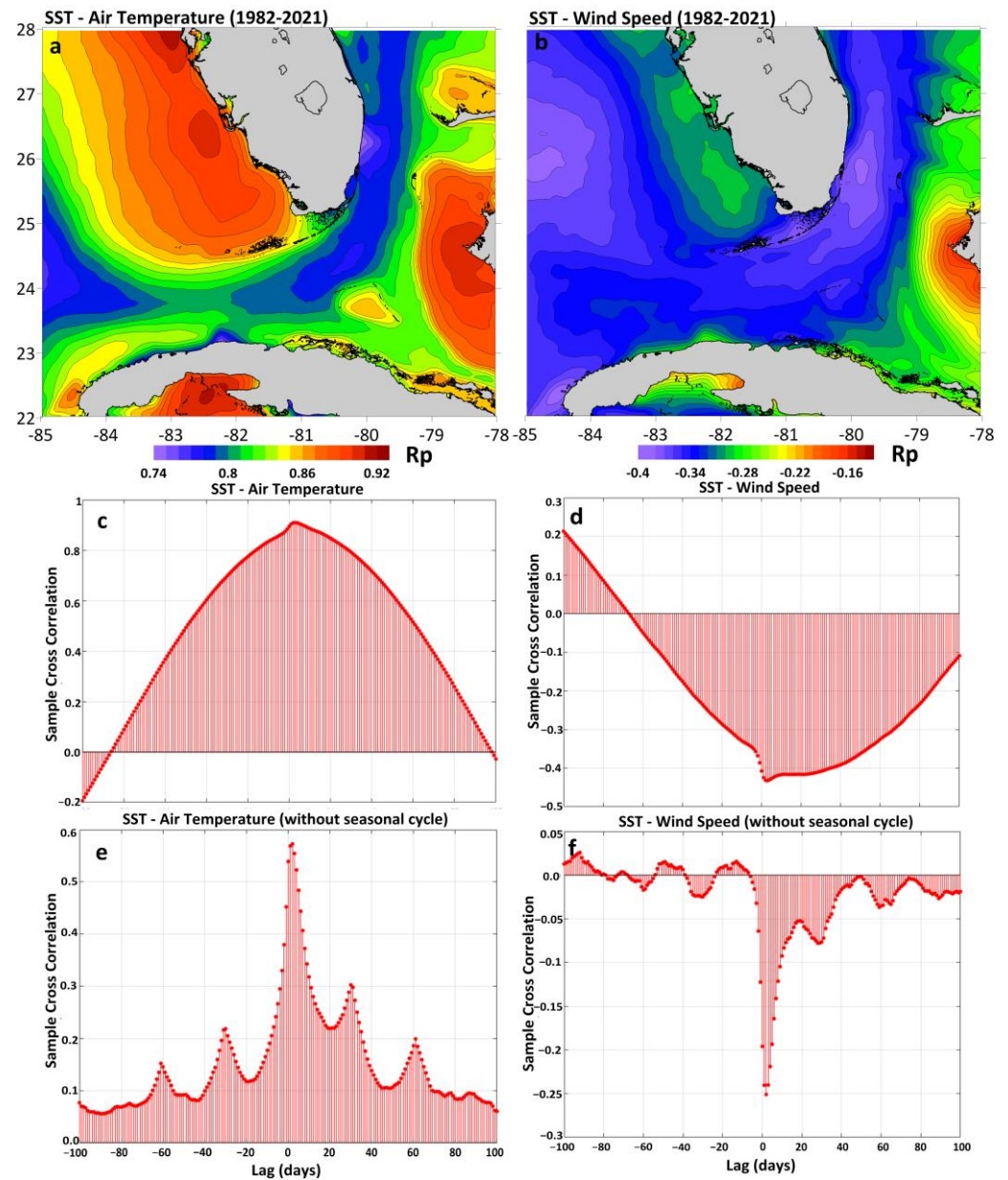

Figure 10. Horizontal distribution of Pearson correlations coefficients (R_P) derived between (**a**) the daily Sea Surface Temperature (SST; satellite observations) and air temperature (ERA 5), and (**b**) the SST and wind speed (ERA5) data over the entire study area and period (1982–2021). Cross correlation between SST and air temperature, and SST and wind speed with (**c**,**d**), and without (**e**,**f**) the seasonal cycle, respectively. The *y*- and *x*-axes represent the Pearson correlation coefficients and lag (days) between each pair of timeseries, respectively.

The wind speed also contributes to the variability of the SST, showing negative Pearson coefficients (counter-correlation) over all areas (Figure 10b). High SST anomalies usually coincide with weak wind anomalies throughout the study period. The strongest impact of the wind on SST was detected over the broader Miami area (25–26° N) with correlation coefficients close to −0.40. The majority of the Straits of Florida showed correlation coefficients around −0.35, while the smallest values were computed for the Bahamas, where the air temperature effect is stronger (Figure 10a). Relatively weak correlation ($R_P = -0.29$) was

also detected along the western coast of Florida and north of the Florida Keys. Generally, the impact of the wind on SST is weaker and more spatially homogenous compared to the air temperature effect. The general correlation coefficient, derived from all daily values is approximately $R_p = -0.43$ and reveals the same small lag (~3 days) for seasonal (Figure 10d) and non-seasonal (Figure 10f) timeseries. The correlation coefficient of the non-seasonal correlations, which is derived from variations related to extreme events is smaller and equal to -0.25.

The mean monthly evolution of the SST (seasonal cycle removed) at specific coastal areas (insert maps in Figure 8) shows statistically significant increasing trends for all regions ($p_{values} < 0.01$; Figure 11). The respective air temperature anomalies (seasonal cycle removed) reveal a similar variability to the SST anomalies, leading to high positive correlation coefficients ($R_p > 0.60$).
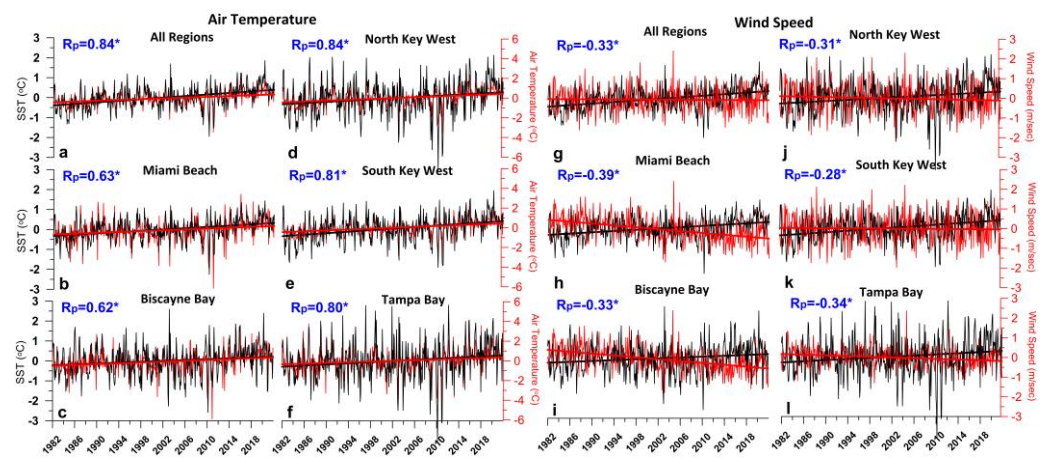

Figure 11. Monthly evolutions, without the seasonal cycle, of the Sea Surface Temperatures (SST anomaly, black line, °C), air temperature (red line in upper panels; °C) and wind speed (red line in lower panels; m/s), averaged over: (**a,g**) All Regions (entire study domain); (**b,h**) Miami Beach; (**c,i**) Biscayne Bay; (**d,j**) North Key West; (**e,k**) South Key West; (**f,l**) Tampa Bay, over the 1982–2021 period (areas marked in Figure 8). The linear trends and the Pearson correlation coefficients (R_p) for each case are shown. The asterisks (*) indicate statistically significant correlations of 99%.

The stronger impact of air temperature was observed at areas where the effects of the Gulf's mesoscale ocean dynamics are weaker, such as Tampa Bay in the west Florida coast (Figure 11f), and Key West (Figure 11d,e). The general correlation is around 0.84 (Figure 11a) but the Miami Beach and Biscayne Bay areas are characterized by significantly weaker correlations ($R_p < 0.65$; Figure 11b,c). The latter showed slightly stronger correlation between the measured atmospheric temperature at Buoy FWYF1 and SST (Figure 12a). The respective correlation between the SST and the air temperature is weaker in Miami Beach ($R_p = 0.81$; Figure 12b). The correlation without the seasonal cycle in Biscayne Bay ($R_p = 0.40$) is double than the respective correlation in Miami Beach ($R_p = 0.20$). The linear regression between the two variables is closer to the x = y identity line for the enclosed basin of Biscayne Bay. This suggests that factors other than atmospheric conditions also control the processes impacting SST and MHW there (see Section 4.2). It is noted that these Pearson coefficients are derived from monthly means and, therefore, the general value (Figure 11a) is different from the one derived from daily values to estimate the lag between the two time series (Figure 10e; $R_p = 0.57$). The wind speed interannual trends are negative at all areas with smaller correlation coefficients between the wind speed and the SST anomalies compared to the ones correlating air temperature with SST. These coefficients are similar between the coastal areas, in agreement with the spatial distribution presented in Figure 10b. The highest values at central EFS were derived for Miami Beach, where the air temperature conditions showed the weakest impact on SST among all study coastal

areas. Moreover, very strong decreasing trends of wind speed were computed for both Miami Beach and Biscayne Bay, contributing to the increasing interannual trends of SST.
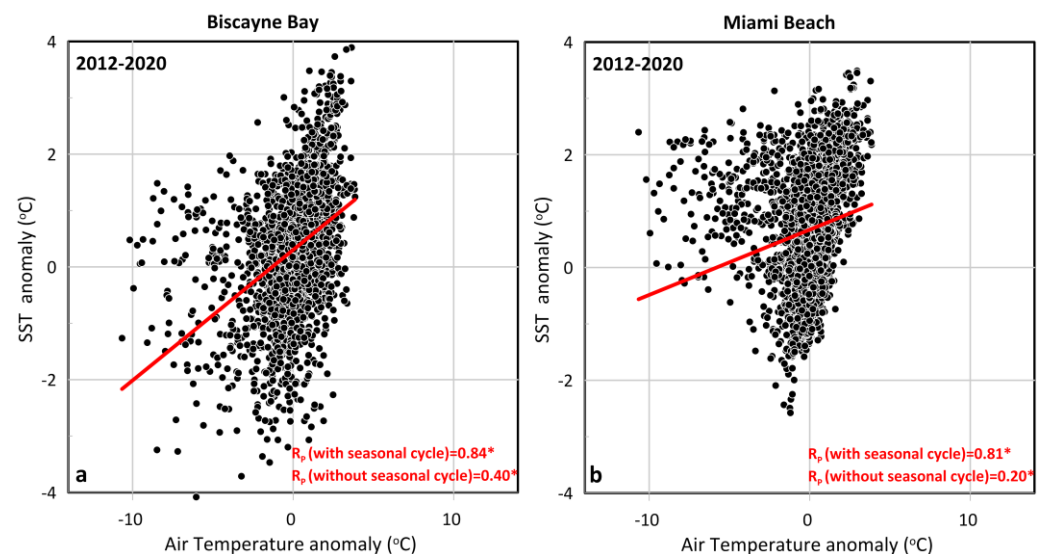

Figure 12. Scatter diagram of daily SST and air temperature anomaly (seasonal cycle excluded), derived for (**a**) Biscayne Bay, and (**b**) Miami Beach covering the 2012–2020 period. The air temperature measurements were collected at the NDBC FWYF1 station located at the coastal area of Miami (Figure 1). The linear regressions (red lines) and the correlation coefficients (R_p) with and without the seasonal cycle are also shown. The asterisk (*) indicates that the hypothesis that the correlation is statistically significant is true (99% MK trend test: $p_{value} < 0.01$).

4.2. Ocean Dynamics Impact on the Temperature and MHW Variability of the Coastal Zone

We showed that the smallest impact of air temperature on the water temperature was detected along the eastern coasts of Florida, and specifically around the broader Miami urban area (Figures 10a and 11). Although the areas of Miami Beach and Biscayne Bay showed similar correlations between atmospheric conditions (air temperature and winds) and SST variability, the MHWs (7.2 MHW/decade for Biscayne Bay and 10 MHW/decade for Miami Beach) and SST (0.1 °C/decade for Biscayne Bay and 0.15 °C/decade for Miami Beach) trends showed significant differences between the two areas (Table 2). Figure 13 presents the mean annual position of the FC as it flows northward along the Straits of Florida at latitude 26° N from 2012 until 2020, carrying warmer Caribbean waters. The FC is known to meander between Florida and the Bahamas; the position of its axis has been calculated here as the 20 °C temperature contour line at 150 m along 26° N [26,28], based on the 9-year FKEYS-HYCOM model archives.

There is a clear interannual trend of the FC shift toward the eastern Florida coast, moving to the nearest shore location in 2019 (79.78° W; Figure 13). The furthest offshore positions (easternmost) were computed for 2012. The mean annual SST anomaly and the mean annual number of MHWs showed increasing trends at both Biscayne Bay (Figure 13a) and Miami Beach (Figure 13b). However, the interannual variations of the mean SST and MHW number for Miami Beach follow the FC variability, indicating stronger FC relation to the ocean temperature variability over this area, which is more exposed to the offshore ocean dynamics, compared to the enclosed Biscayne Bay. This result may explain the weaker effect of atmospheric temperature on SST over Miami Beach (Figure 12b) compared to Biscayne Bay (Figure 12a).
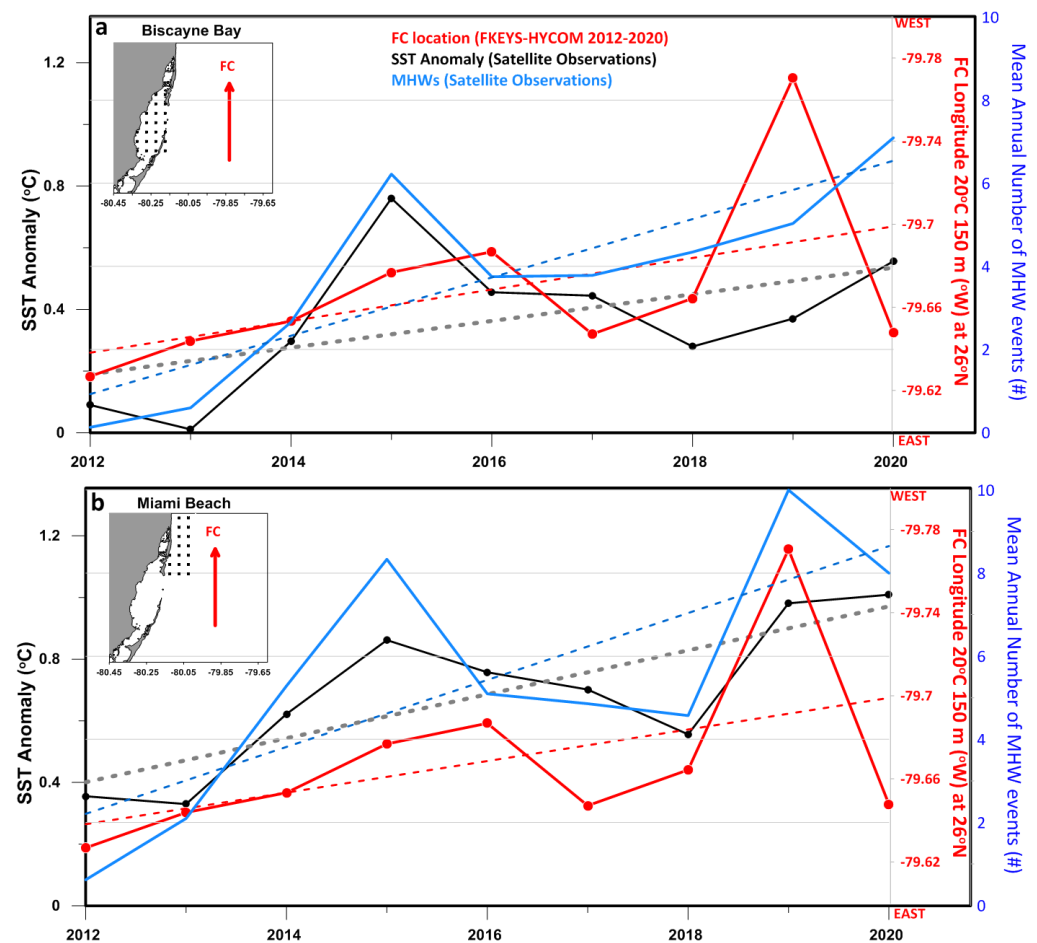
Figure 13. Annual mean of SST anomaly (black line), mean annual number of MHW events (blue line), and Florida Current (FC) longitude based on the 20 °C temperature contour line at 150 m along 26° N that is derived from the FKEYS-HYCOM numerical simulations for (**a**) Biscayne Bay, and (**b**) Miami Beach during the 2012–2020 period. The maps in the inserts represent the area used to estimate the SST anomaly and the MHW events. The linear trend (dashed line) for each case is also presented.

The highest number of MHWs at Miami Beach (Figure 13b) was computed for 2019 (10) following a large drop in 2018 (5), when the FC was further away from the Florida coast (79.66° W); the peak of 2019 and the MHW duration (100 days) were the highest during the entire 40-year period (Figure 8b). On the contrary, Biscayne Bay revealed its highest MHW number in 2020, when the warm FC was away from the coast (Figure 13a). The FC seasonal variability is characterized by more onshore positions during winter and autumn months and more offshore shifts during summer (Figure 14a). This finding agrees with the distribution of the high 90th percentiles over the Straits of Florida during winter and the lower levels than the WFS and EFS areas during the summer months due to the FC evolution that controls the distribution of physical properties over the Straits (Figure 4; Section 3.3).

We focus on Miami Beach to investigate the temperature variability and ocean dynamics over this coastal urban region during 2018 (weak formation) and 2019 (extensive formation). The evolutions of the SST anomaly averaged over the coastal region for the two years are presented in Figure 14b. There is a clear difference of more than 0.4 °C between the 2018 and 2019 timeseries (Figure 14b). The SST with the seasonal cycle (Figure 14c) also showed higher values in 2019, exceeding the monthly 90th percentile several times during the year justifying the high number of MHWs detected during 2019 (Figures 8b and 13b). The westward shift of the FC was apparent throughout the entire year of 2019,

compared to 2018 (Figure 14a); the mean FC longitude was 79.77° W in 2019 and 79.66° W in 2018, while the 6th order polynomial fits between the two years, gradually diverging by the end of the year. March of 2019 was characterized by successive peaks of westward FC shifts (Figure 14a) that coincided with the SST anomaly increases (Figure 14b) above the monthly threshold of the 90th percentile (Figure 14c). Moreover, the gradual movement of the FC towards Miami Beach during the first half of November 2019 (Figure 14a) increased the SST anomaly in values higher than 2 °C, resulting in continuous high levels of SST that exceeded the 90th percentile of November for more than 15 days (formation of a long MHW event). The spatial distributions of the total number of MHW events in 2019 and the respective total durations in days over the broader Miami area are presented in Figure 15b,d, respectively. The MHWs east of Miami Beach, were more than 10, exceeding the 100 days duration, while Biscayne Bay showed significantly lower numbers.
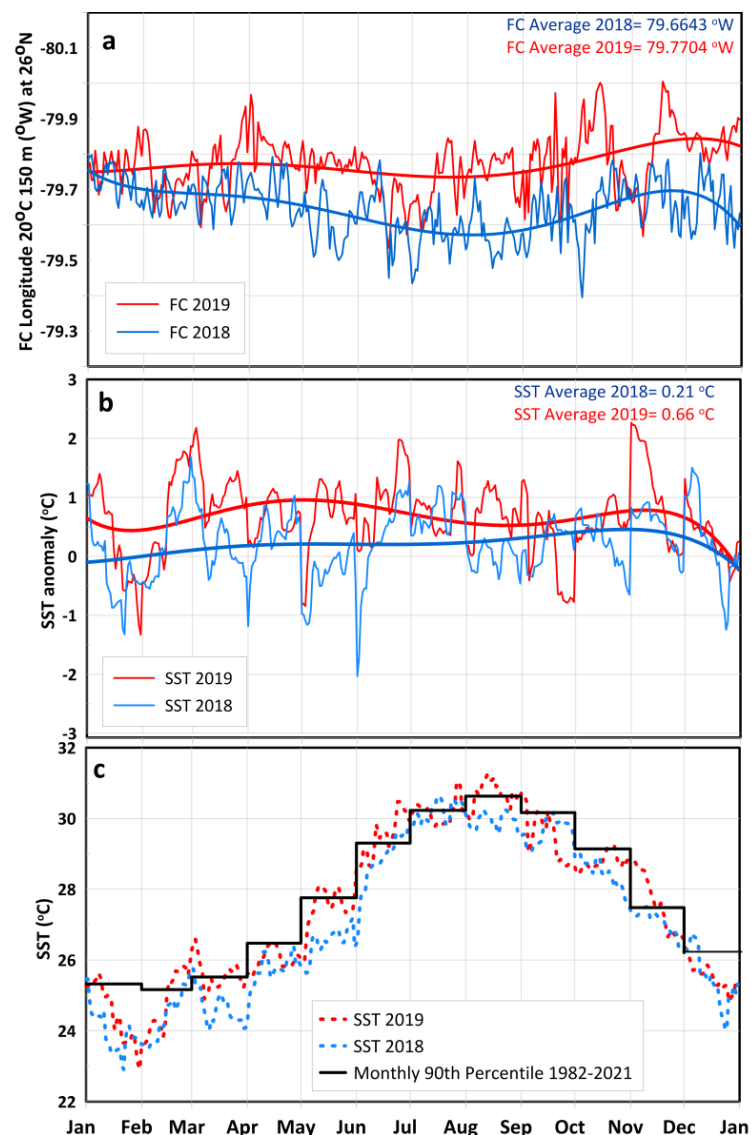

Figure 14. Daily evolution of (**a**) the Florida Current (FC) longitude, based on the 20 °C temperature contour line at 150 m along 26° N that is derived from the FKEYS-HYCOM numerical simulations, the Miami Beach Sea Surface Temperature (**b**) without (SST anomaly) and (**c**) with the seasonal cycle (satellite observations) for 2018 (blue lines) and 2019 (red lines). The mean monthly 90th percentiles of SST derived for the Miami Beach coastal area from the 1982–2021 satellite dataset (black line) is presented in (**c**). The 6th order polynomial fits and the annual means of the FC longitude and the SST for each year are also shown.
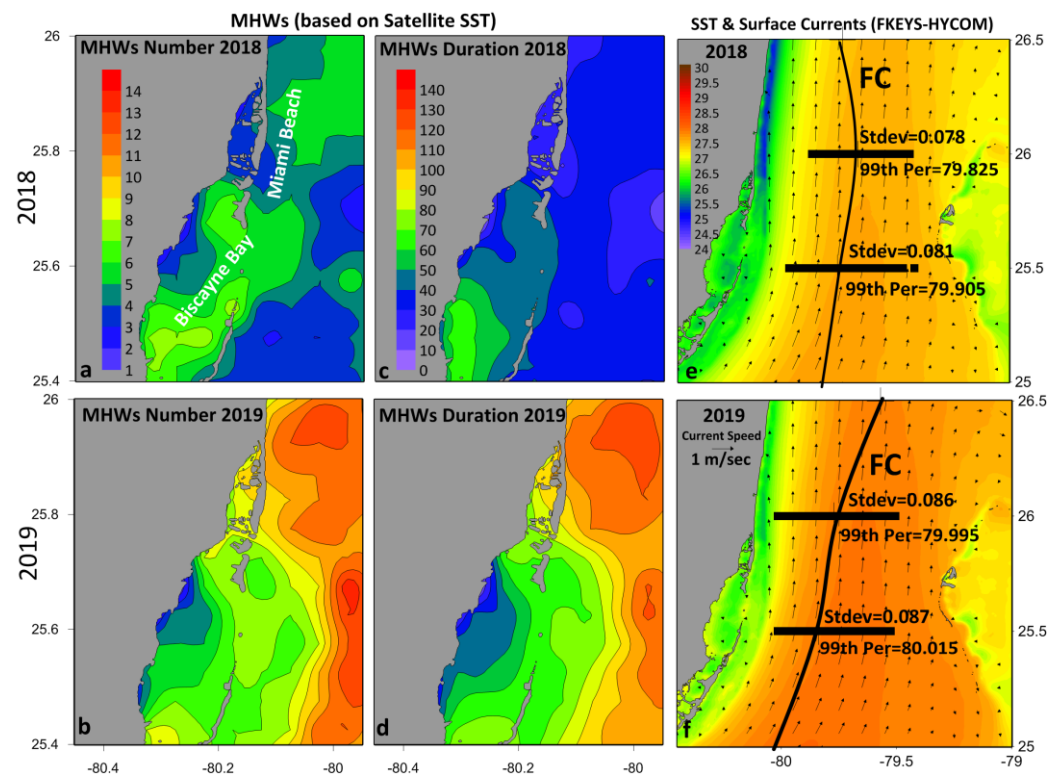
Figure 15. Horizontal distribution of (**a**,**b**) MHWs number, (**c**,**d**) MHW duration for 2018 and 2019, derived from the satellite SST dataset over Biscayne Bay and Miami Beach. The SST, the surface currents and the position of the FC front (black lines along the Straits), derived from the FKEYS-HYCOM simulations are averaged over (**e**) 2018 and (**f**) 2019. The Miami Beach and Biscayne Bay areas are marked in (**a**). The horizontal thick lines consists of all daily FC positions at 25.5° N and 26° N for years (**e**) 2018 and (**f**) 2019 together with the Standard Deviation (Stdev) and 99th Percentile (Per) of the annual longitude positions.

We examine the relationship between coastal MHWs and ocean influence, which is suggested by the SST and FC variability discussed above for 2018 and 2019. The highest number of MHWs were observed along the Miami Beach in 2019 (Figure 15b) showing total duration of more than 110 days, especially over the northern areas (Figure 15d). On the contrary, the same area revealed very small durations in 2018 (<40 days; Figure 15c) associated with very low number of events (<8; Figure 15a). The warm waters of the northward FC (>28 °C) affected the temperature levels along the coastline (>26 °C) during 2019 (Figure 15f). In 2018, the surface waters along the coast of Miami Beach were significantly colder (<25 °C), while Biscayne Bay waters were warmer (>26 °C; Figure 15e). The overall position of the FC and the respective daily values at offshore Miami Beach (26° N) and Biscayne Bay (25.5° N) are presented in Figure 15e (2018) and Figure 15f (2019). The annual deviation of the FC longitudes is larger in 2019 than in 2018, when the FC flowed more offshore (eastward) at the area south of the 26° N latitude. In 2019, the 99th percentile of the FC longitude at 26° N was 79.995° W (Figure 15f), approximately 0.2 degrees more to the west (onshore) than the respective 2018 percentile (79.825° W; Figure 15e); this was the area where the highest MHW frequencies of 2019 occurred (Figure 15b,d). The 99th percentile at 25.5° N was 80.015° W for 2019 and 79.905° W for 2018. Both Miami Beach and Biscayne Bay revealed similar MHW distributions in 2018 (Figure 15a,c), when the FC flowed further offshore from the coast (Figure 15e), supporting the SST reduction along the Miami Beach coasts. It is shown that the SST and MHW variability, especially over the more exposed coastal areas of Miami Beach, are largely controlled by ocean dynamics (in addition to atmospheric conditions), related to the evolution and zonal (longitudinal) position of the warm FC over the northern Straits of Florida.

4.3. Implications of MHWs on the Sustainability of the Coastal Natural and Urban Environments

MHWs, similarly to the atmospheric heat waves [57,58], have disastrous impacts on the ecosystem affecting the health of marine species [13]. Increasing ocean temperatures over South Florida induce extended coral bleaching, fish diseases, losses of sponges and other marine plants and animals, decreased biodiversity, changes in the distribution of native and invasive exotic marine species, changes in food webs, and increased occurrence of harmful algal blooms and hypoxia [59]. The increase of the MHW frequency and duration at global scale during the last century caused widespread loss of habitat-forming species such as corals [60]. Coral bleaching is strongly related to extreme temperature events, when the algae living on corals escape from the heat, leaving the corals white [61,62]. Other environmental factors (e.g., solar radiation, wind speed and direction, currents, stratification) additionally deteriorate the resilience of the corals. The recorded coral reef decline in the Florida Keys is strongly related to the increasing thermal stress due to ocean warming from climate change [55]. The most lethal coral-disease incident ever recorded on a contemporary coral reef occurred over southeast Florida during 2014–2015 [63], when very high occurrence frequencies of MHWs with total durations above 100 days were computed (Figure 8). Precht et al. [63] associated the coral losses with unusually warm-winter and spring temperatures followed by an anomalously warm summer, in agreement with our satellite-derived results that showed high minimum (winter) SST values (Figure 3c) in 2014 and high maximum (summer) values in 2015 (Figure 3b). Besides 2014 and 2015, Manzello et al. [64] reported one more major bleaching event at Cheeca Rocks, located between Marathon and Key Largo, in 2011, when increased number of MHWs was also computed (Figure 8), associated with the increased 99th SST percentile of that year (>30.5 °C; Figure 3b). The peak of MHWs in 1998 (Figure 6a), associated with the high SST (>30.8 °C for 99th percentile; Figure 3b, and >26.5 for mean SST; Figure 3a) of the recent El Nino, affected the Florida Keys and, in combination to a rise in the growth and reproduction of microbial pathogens, favored the coral bleaching and mortality in the Florida Keys [65]. The high SST levels of 1998 were also responsible for the formation of MHWs in Biscayne Bay (Figure 8c), affecting the coral distribution within the enclosed bay [66]. The increasing number of MHWs observed (e.g., Figure 8e–g) in the Florida Keys between 1996–1999 led to the reduction of the mean percent of live coral cover in the Florida Keys National Marine Sanctuary during the same years (approximately 5% reduction; [67]); the bleaching and cover decline of M. complanata were greatest from 1998 to 1999 that has not recovered since then. The thermal stress due to the high temperatures of 2015 was also apparent on seagrass, adding to its mortality in the Florida Bay ecosystem, similarly to another period of seagrass die-off during 1987–1991 [17], when MHWs were also increased (Figure 6a). Our findings suggest that the Florida Bay region is a "hot spot" of MHWs, revealing significant large number of events (>130; Figure 7c) with long durations (>1100 days; Figure 7d) during the entire study period. Mangrove species along the coastal zone are also controlled by climate-related factors such as air and soil temperature which correlates with SST due to tidal inundations [68,69].

MHWs, and especially the recorded increasing trends of their event number and duration, can also affect the well-being of coastal communities. The results are significant political and socio-economic ramifications, such as effects on recreation and tourism (e.g., impacts on coral reefs), aquaculture or important fishery species [13]. The biotic and habitat loss of corals due to ocean warming may result in severe economic and social losses [70]. Birkeland [71] estimated that Florida's reefs produce approximately USD 1.6 billion annually in tourism value. Chen et al. [72], based on different RCP climate scenarios during the 21st century, estimated that the future global coral reef recreational and tourism value loss may range from USD 1.88 to USD 12.02 billion annually. Changing conditions can also help invasive alien species to spread, which can be devastating for marine food webs as reported by the International Union for Conservation of Nature (IUCN; https://www.iucn.org/resources/issues-brief/marine-heatwaves, accessed on 1 September 2022). Protracted high ocean temperatures and the associated MHWs may

also affect several economically important species like lobster [73] and snow crab [74]. Moreover, the mortality and destruction of those species that contribute to the coastal defense against erosion and flooding, indirectly affect coastal communities' socioeconomic conditions. Coral reefs [75] and mangroves [76] may reduce the wave energy that reaches the shore and minimize the impact of hurricanes and the associated storm surge, protecting coastal economic activity [77,78]. The incoming waves can be reduced between 50% to 100% using mangroves of 500 m width [79] and up to 97% over coral reefs [80], maintaining the sandy beaches [81].

The severe MHW events recorded posterior to 2015, and especially in 2019 and 2020 (Figure 6), at all coastal areas (Figure 8) might also have further affected the natural and human system of South Florida, requiring more interdisciplinary studies to estimate the impact of the strong increasing trends of the ocean temperature and the associated MHW formations. It is essential to develop a better understanding of how the MHWs impact these tropical ecosystems and the people that rely on these ecosystems for their livelihood. Urban planning for sustainable development in South Florida's coastal cities must take into account MHW trends.

5. Conclusions

The formation of Marine Heat Waves (MHWs) over natural and urban coastal environment of South Florida, related to the increasing trends of Sea Surface Temperature (SST) at the adjacent ocean waters, has been investigated with the use of high-resolution satellite-derived SST data during 1982–2021. We showed that the SST daily fields covering the 40-year period are suitable to estimate the temperature distribution over the topographically complicated South Florida coastal region and to examine the formation of MHW events.

The interannual positive trend of the MHWs is 0.75 events/decade with 7.4 days/decade duration increase and is associated with the general increasing SST trend over the entire region (0.19 °C/decade), following the respective atmospheric temperature (0.21 °C/decade) and the heat flux (~5000 J/m^2/decade) increases. The period between 2013–2021 revealed the highest SST levels, during both winter and summer, while the increasing trends of the previous period were mainly associated with summer extremes. Although the majority of the MHWs of South Florida are "moderate" events, based on the Hobday et al. (2018) categorization, in the years after 2015, "severe" MHWs were also formed. Specifically, the seven most recent years (2015–2021) were characterized by the strongest formation of MHWs and strong peaks in 2015, 2019 and 2020 with more than 8 events/year and approximately 70 to 110 days/year duration in total. During the last decade, the annual variance was also smaller than the previous period confirming the general warming of the ocean throughout all seasons (both winter and summer months).

The south WFS and Florida Bay showed the highest number of events during the 40-year period, but significantly long MHWs also occurred at the northern parts of WFS. The interannual trends of MHWs were though weak over coastal WFS, with small increasing slopes at the coastal areas of Tampa and Fort Myers. The Dry Tortugas and Florida Keys, especially along the Straits of Florida (southern coasts) revealed very strong increasing trends. Miami Beach is also characterized by strong interannual trends (1.1 events/decade and 10 days/decade) compared to the enclosed basin of Biscayne Bay. Although the atmospheric conditions mainly affected the formation of MHWs over all coastal regions, the eastern Florida coasts and especially the most exposed (e.g., Miami Beach) are also controlled by ocean dynamics, related to the warm Florida Current (FC). The evolution of the FC close to the eastern coasts is a pre-condition of MHW formation, while its offshore shift away from the coast results to colder coastal waters, unfavorable for MWH formation. The colder waters have been detected in the central Western Florida Shelf (WFS) between the months of January to March, while the Eastern Florida Shelf (EFS), south of Florida Keys, and the southwestern WFS include the warmest coastal areas with the highest interannual increasing trends.

Several disastrous events on the biotic environment of South Florida are related to unusual temperature extremes and coincide with the peaks of MHWs. Coral Bleaching is strongly related to MHW events over the Florida Reef Tract. More investigation of the effect of ocean physical properties and their variability on the biochemical characteristics and the resilience of species, sensitive to heat stress, is essential. The indirect but strong impact of MHWs, and especially the increasing trends detected during the last decades, on the sustainability of urban coastal system have not been investigated in detail yet and require more interdisciplinary research combining different branches of science (environmental and socioeconomic). The effects of the most recent extreme events (2019–2020) on the ecosystem require the conduction of focused studies, especially over the coastal areas of South Florida with the highest occurrence frequencies of MHW formation. Our results may aid policy makers because they highlight that the conservation and restoration efforts of natural barriers such as coral reefs and mangroves are essential in coastal areas of South Florida to protect economic activity against tropical cyclones. This is crucial in the context of climate change, as besides MHWs, tropical storms and hurricanes are expected to increase in intensity [82], enhancing the potential for catastrophic effects on coastal natural and urban environments.

References

1. Hobday, A.J.; Alexander, L.V.; Perkins, S.E.; Smale, D.A.; Straub, S.C.; Oliver, E.C.; Benthuysen, J.A.; Burrows, M.T.; Donat, M.G.; Feng, M.; et al. A hierarchical approach to defining marine heatwaves. *Prog. Oceanogr.* **2016**, *141*, 227–238. [CrossRef]
2. Hobday, A.J.; Oliver, E.C.; Gupta, A.S.; Benthuysen, J.A.; Burrows, M.T.; Donat, M.G.; Holbrook, N.J.; Moore, P.J.; Thomsen, M.S.; Wernberg, T.; et al. Categorizing and naming marine heatwaves. *Oceanography* **2018**, *31*, 162–173. [CrossRef]
3. Kent, E.C.; Taylor, P.K. Toward estimating climatic trends in SST. Part I: Methods of measurement. *J. Atmos. Ocean. Technol.* **2006**, *23*, 464–475. [CrossRef]
4. Garrabou, J.; Coma, R.; Bensoussan, N.; Bally, M.; Chevaldonné, P.; Cigliano, M.; Díaz, D.; Harmelin, J.G.; Gambi, M.C.; Kersting, D.K.; et al. Mass mortality in Northwestern Mediterranean rocky benthic communities: Effects of the 2003 heat wave. *Glob. Change Biol.* **2009**, *15*, 1090–1103. [CrossRef]
5. Pearce, A.F.; Feng, M. The rise and fall of the "marine heat wave" off Western Australia during the summer of 2010/2011. *J. Mar. Syst.* **2013**, *111*, 139–156. [CrossRef]
6. Wernberg, T.; Smale, D.A.; Tuya, F.; Thomsen, M.S.; Langlois, T.J.; De Bettignies, T.; Bennett, S.; Rousseaux, C.S. An extreme climatic event alters marine ecosystem structure in a global biodiversity hotspot. *Nat. Clim. Change* **2013**, *3*, 78–82. [CrossRef]
7. Mills, K.E.; Pershing, A.J.; Brown, C.J.; Chen, Y.; Chiang, F.S.; Holland, D.S.; Lehuta, S.; Nye, J.A.; Sun, J.C.; Thomas, A.C.; et al. Fisheries management in a changing climate: Lessons from the 2012 ocean heat wave in the Northwest Atlantic. *Oceanography* **2013**, *26*, 191–195. [CrossRef]
8. Di Lorenzo, E.; Mantua, N. Multi-year persistence of the 2014/15 North Pacific marine heatwave. *Nat. Clim. Change* **2016**, *6*, 1042–1047. [CrossRef]
9. Oliver, E.C.; Benthuysen, J.A.; Bindoff, N.L.; Hobday, A.J.; Holbrook, N.J.; Mundy, C.N.; Perkins-Kirkpatrick, S.E. The unprecedented 2015/16 Tasman Sea marine heatwave. *Nat. Commun.* **2017**, *8*, 16101. [CrossRef]
10. Darmaraki, S.; Somot, S.; Sevault, F.; Nabat, P. Past variability of Mediterranean Sea marine heatwaves. *Geophys. Res. Lett.* **2019**, *46*, 9813–9823. [CrossRef]

11. Ibrahim, O.; Mohamed, B.; Nagy, H. Spatial variability and trends of marine heat waves in the eastern mediterranean sea over 39 years. *J. Mar. Sci. Eng.* **2021**, *9*, 643. [CrossRef]

12. Androulidakis, Y.S.; Krestenitis, Y.N. Sea Surface Temperature Variability and Marine Heat Waves over the Aegean, Ionian, and Cretan Seas from 2008–2021. *J. Mar. Sci. Eng.* **2022**, *10*, 42. [CrossRef]

13. Frölicher, T.L.; Laufkötter, C. Emerging risks from marine heat waves. *Nat. Commun.* **2018**, *9*, 650. [CrossRef]

14. Oliver, E.C.; Donat, M.G.; Burrows, M.T.; Moore, P.J.; Smale, D.A.; Alexander, L.V.; Benthuysen, J.A.; Feng, M.; Sen Gupta, A.; Hobday, A.J.; et al. Longer and more frequent marine heatwaves over the past century. *Nat. Commun.* **2018**, *9*, 1324. [CrossRef]

15. Lirman, D.; Ault, J.S.; Fourqurean, J.W.; Lorenz, J.J. The coastal marine ecosystem of south Florida, United States. In *World Seas: An Environmental Evaluation*; Academic Press: Cambridge, MA, USA, 2019; pp. 427–444.

16. Kuffner, I.B.; Lidz, B.H.; Hudson, J.H.; Anderson, J.S. A century of ocean warming on Florida Keys coral reefs: Historic in-situ observations. *Estuaries Coasts* **2015**, *38*, 1085–1096. [CrossRef]

17. Carlson, D.F.; Yarbro, L.A.; Scolaro, S.; Poniatowski, M.; McGee-Absten, V.; Carlson, P.R., Jr. Sea surface temperatures and seagrass mortality in Florida Bay: Spatial and temporal patterns discerned from MODIS and AVHRR data. *Remote Sens. Environ.* **2018**, *208*, 171–188. [CrossRef]

18. Mann, H.B. Nonparametric tests against trend. *Econom. J. Econom. Soc.* **1945**, *13*, 245–259. [CrossRef]

19. Kendall, M. *Rank Correlation Measures*; Charles Griffin: London, UK, 1975.

20. Liu, Y.; Weisberg, R.H.; He, R. Sea surface temperature patterns on the West Florida Shelf using growing hierarchical self-organizing maps. *J. Atmos. Ocean. Technol.* **2006**, *23*, 325–338. [CrossRef]

21. Soto, I.M.; Muller Karger, F.E.; Hallock, P.; Hu, C. Sea surface temperature variability in the Florida Keys and its relationship to coral cover. *J. Mar. Biol.* **2011**, *2011*, 981723. [CrossRef]

22. Barnes, B.B.; Hu, C.; Muller-Karger, F. An improved high-resolution SST climatology to assess cold water events off Florida. *IEEE Geosci. Remote Sens. Lett.* **2011**, *8*, 769–773. [CrossRef]

23. Colella, M.A.; Ruzicka, R.R.; Kidney, J.A.; Morrison, J.M.; Brinkhuis, V.B. Cold-water event of January 2010 results in catastrophic benthic mortality on patch reefs in the Florida Keys. *Coral Reefs* **2012**, *31*, 621–632. [CrossRef]

24. Stith, B.M.; Slone, D.H.; De Wit, M.; Edwards, H.H.; Langtimm, C.A.; Swain, E.D.; Soderqvist, L.E.; Reid, J.P. Passive thermal refugia provided warm water for Florida manatees during the severe winter of 2009–2010. *Mar. Ecol. Prog. Ser.* **2012**, *462*, 287–301. [CrossRef]

25. Johns, W.E.; Schott, F. Meandering and transport variations of the Florida Current. *J. Phys. Oceanogr.* **1987**, *17*, 1128–1147. [CrossRef]

26. Kourafalou, V.H.; Kang, H. Florida Current meandering and evolution of cyclonic eddies along the Florida Keys Reef Tract: Are they interconnected? *J. Geophys. Res. Ocean.* **2012**, *117*. [CrossRef]

27. Kourafalou, V.; Androulidakis, Y.; Le Hénaff, M.; Kang, H. The dynamics of Cuba anticyclones (CubANs) and interaction with the Loop Current/Florida Current system. *J. Geophys. Res. Ocean.* **2017**, *122*, 7897–7923. [CrossRef]

28. Androulidakis, Y.; Kourafalou, V.; Le Hénaff, M.; Kang, H.; Ntaganou, N.; Hu, C. Gulf Stream evolution through the Straits of Florida: The role of eddies and upwelling near Cuba. *Ocean. Dyn.* **2020**, *70*, 1005–1032. [CrossRef]

29. Lee, T.N.; Leaman, K.; Williams, E.; Berger, T.; Atkinson, L. Florida Current meanders and gyre formation in the southern Straits of Florida. *J. Geophys. Res.* **1995**, *100*, 8607–8620. [CrossRef]

30. Kourafalou, V.H.; Androulidakis, Y.S.; Kang, H.; Smith, R.H.; Valle-Levinson, A. Physical connectivity between Pulley Ridge and Dry Tortugas coral reefs under the influence of the Loop Current/Florida Current system. *Prog. Oceanogr.* **2018**, *165*, 75–99. [CrossRef]

31. Fratantoni, P.S.; Lee, T.N.; Podesta, G.P.; Muller-Karger, F. The influence of Loop Current perturbations on the formation and evolution of Tortugas eddies in the southern Straits of Florida. *J. Geophys. Res. Ocean.* **1998**, *103*, 24759–24779. [CrossRef]

32. Le Hénaff, M.; Kourafalou, V.H.; Morel, Y.; Srinivasan, A. Simulating the dynamics and intensification of cyclonic Loop Current frontal eddies in the Gulf of Mexico. *J. Geophys. Res.* **2012**, *117*, C02034. [CrossRef]

33. Weisberg, R.H.; Li, Z.; Muller-Karger, F. West Florida shelf response to local wind forcing: April 1998. *J. Geophys. Res. Ocean.* **2001**, *106*, 31239–31262. [CrossRef]

34. Weisberg, R.H.; He, R. Local and deep-ocean forcing contributions to anomalous water properties on the West Florida Shelf. *J. Geophys. Res. Ocean.* **2003**, *108*. [CrossRef]

35. Weisberg, R.H.; Liu, Y.; Mayer, D.A. West Florida Shelf mean circulation observed with long-term moorings. *Geophys. Res. Lett.* **2009**, *36*. [CrossRef]

36. Weisberg, R.H.; Black, B.D.; Li, Z. An upwelling case study on Florida's west coast. *J. Geophys. Res. Ocean.* **2000**, *105*, 11459–11469. [CrossRef]

37. Weisberg, R.H.; Zheng, L.; Liu, Y. West Florida shelf upwelling: Origins and pathways. *J. Geophys. Res. Ocean.* **2016**, *121*, 5672–5681. [CrossRef]

38. Taylor, C.B.; Stewart, H.B., Jr. Summer upwelling along the east coast of Florida. *J. Geophys. Res.* **1959**, *64*, 33–40. [CrossRef]

39. Smith, N.P. Temporal and spatial characteristics of summer upwelling along Florida's Atlantic shelf. *J. Phys. Oceanogr.* **1983**, *13*, 1709–1715. [CrossRef]

40. Duever, M.J.; Meeder, J.F.; Meeder, L.C.; McCollom, J.M. The climate of south Florida and its role in shaping the Everglades ecosystem. In *Everglades: The Ecosystem and Its Restoration*; CRC Press: Boca Raton, FL, USA, 1994; pp. 225–248.

41. Malmstadt, J.C.; Elsner, J.B.; Jagger, T.H. Risk of strong hurricane winds to Florida cities. *J. Appl. Meteorol. Climatol.* **2010**, *49*, 2121–2132. [CrossRef]
42. Sponaugle, S.; Paris, C.; Walter, K.; Kourafalou, V.H.; Alessandro, E.D. Observed and modeled larval settlement of a reef fish to the Florida Keys. *Mar. Ecol. Prog. Ser.* **2012**, *453*, 201–212. [CrossRef]
43. Vaz, A.C.; Paris, C.B.; Olascoaga, M.J.; Kourafalou, V.H.; Kang, H. The perfect storm: Match-mismatch of bio-physical events drives larval reef fish connectivity between Pulley Ridge and the Florida Keys. *Cont. Shelf Res.* **2016**, *125*, 136–146. [CrossRef]
44. Good, S.; Fiedler, E.; Mao, C.; Martin, M.J.; Maycock, A.; Reid, R.; Roberts-Jones, J.; Searle, T.; Waters, J.; While, J.; et al. The current configuration of the OSTIA system for operational production of foundation sea surface temperature and ice concentration analyses. *Remote Sens.* **2020**, *12*, 720. [CrossRef]
45. Nagy, H.; Mohamed, B.; Ibrahim, O. Variability of Heat and Water Fluxes in the Red Sea Using ERA5 Data (1981–2020). *J. Mar. Sci. Eng.* **2021**, *9*, 1276. [CrossRef]
46. Bleck, R. An oceanic general circulation model framed in hybrid isopycnic-Cartesian coordinates. *Ocean. Model.* **2002**, *4*, 55–88. [CrossRef]
47. Chassignet, E.P.; Smith, L.T.; Halliwell, G.R.; Bleck, R. North Atlantic simulations with the Hybrid Coordinate Ocean Model (HYCOM): Impact of the vertical coordinate choice, reference pressure, and thermobaricity. *J. Phys. Oceanogr.* **2003**, *33*, 2504–2526. [CrossRef]
48. Halliwell, G.R. Evaluation of vertical coordinate and vertical mixing algorithms in the HYbrid-Coordinate Ocean Model (HYCOM). *Ocean. Model.* **2004**, *7*, 285–322. [CrossRef]
49. Kourafalou, V.H.; Peng, G.; Kang, H.; Hogan, P.J.; Smedstad, O.M.; Weisberg, R.H. Evaluation of Global Ocean Data Assimilation Experiment products on South Florida nested simulations with the Hybrid Coordinate Ocean Model. *Ocean. Dyn.* **2009**, *59*, 47–66. [CrossRef]
50. Metzger, E.J.; Wallcraft, A.J.; Posey, P.G.; Smedstad, O.M.; Franklin, D.S. *The Switchover from NOGAPS to NAVGEM 1.1 Atmospheric Forcing in GOFS and ACNFS*; Naval Research Lab Stennis Detachment Stennis Space Center Ms Oceanography Div: Washington, DC, USA, 2013.
51. Kourafalou, V.H.; De Mey, P.; Le Hénaff, M.; Charria, G.; Edwards, C.A.; He, R.; Herzfeld, M.; Pascual, A.; Stanev, E.V.; Tintoré, J.; et al. Coastal Ocean Forecasting: System integration and evaluation. *J. Oper. Oceanogr.* **2015**, *8* (Suppl. 1), s127–s146. [CrossRef]
52. Holbrook, N.J.; Scannell, H.A.; Sen Gupta, A.; Benthuysen, J.A.; Feng, M.; Oliver, E.C.; Alexander, L.V.; Burrows, M.T.; Donat, M.G.; Hobday, A.J.; et al. A global assessment of marine heatwaves and their drivers. *Nat. Commun.* **2019**, *10*, 2624. [CrossRef]
53. Sanford, E.; Sones, J.L.; García-Reyes, M.; Goddard, J.H.; Largier, J.L. Widespread shifts in the coastal biota of northern California during the 2014–2016 marine heatwaves. *Sci. Rep.* **2019**, *9*, 4216. [CrossRef]
54. Sen, P.K. Estimates of the regression coefficient based on Kendall's tau. *J. Am. Stat. As* **1968**, *63*, 1379–1389. [CrossRef]
55. Manzello, D.P. Rapid recent warming of coral reefs in the Florida Keys. *Sci. Rep.* **2015**, *5*, 16762. [CrossRef]
56. He, R.; Weisberg, R.H. A Loop Current intrusion case study on the West Florida Shelf. *J. Phys. Oceanogr.* **2003**, *33*, 465–477. [CrossRef]
57. Perkins, S.E. A review on the scientific understanding of heatwaves—Their measurement, driving mechanisms, and changes at the global scale. *Atmos. Res.* **2015**, *164*, 242–267. [CrossRef]
58. Breshears, D.D.; Fontaine, J.B.; Ruthrof, K.X.; Field, J.P.; Feng, X.; Burger, J.R.; Law, D.J.; Kala, J.; Hardy, G.E.S.J. Underappreciated plant vulnerabilities to heat waves. *New Phytol.* **2021**, *231*, 32–39. [CrossRef]
59. Florida Oceans and Coastal Council. *The Effects of Climate Change on Florida's Ocean and Coastal Resources*; Report; Florida Oceans and Coastal Council: Tallahassee, FL, USA, 2009.
60. Oliver, J.K.; Berkelmans, R.; Eakin, C.M. Coral bleaching in space and time. In *Coral Bleaching*; Springer: Cham, Switzerland, 2018; pp. 27–49.
61. Hughes, T.P.; Kerry, J.T.; Álvarez-Noriega, M.; Álvarez-Romero, J.G.; Anderson, K.D.; Baird, A.H.; Babcock, R.C.; Beger, M.; Bellwood, D.R.; Berkelmans, R.; et al. Global warming and recurrent mass bleaching of corals. *Nature* **2017**, *543*, 373–377. [CrossRef]
62. Barnes, B.B.; Hallock, P.; Hu, C.; Muller-Karger, F.; Palandro, D.; Walter, C.; Zepp, R. Prediction of coral bleaching in the Florida Keys using remotely sensed data. *Coral Reefs* **2015**, *34*, 491–503. [CrossRef]
63. Precht, W.F.; Gintert, B.E.; Robbart, M.L.; Fura, R.; Van Woesik, R. Unprecedented disease-related coral mortality in Southeastern Florida. *Sci. Rep.* **2016**, *6*, 31374. [CrossRef]
64. Manzello, D.P.; Enochs, I.C.; Kolodziej, G.; Carlton, R.; Valentino, L. Resilience in carbonate production despite three coral bleaching events in 5 years on an inshore patch reef in the Florida Keys. *Mar. Biol.* **2018**, *165*, 99. [CrossRef]
65. Harvell, D.; Kim, K.; Quirolo, C.; Weir, J.; Smith, G. Coral bleaching and disease: Contributors to 1998 mass mortality in Briareum asbestinum (Octocorallia, Gorgonacea). *Hydrobiologia* **2001**, *460*, 97–104. [CrossRef]
66. Lirman, D.; Cropper, W.P. The influence of salinity on seagrass growth, survivorship, and distribution within Biscayne Bay, Florida: Field, experimental, and modeling studies. *Estuaries* **2003**, *26*, 131–141. [CrossRef]
67. Collier, C.; Ruzicka, R.; Banks, K.; Barbieri, L.; Beal, J.; Bingham, D.; Bohnsack, J.A.; Brooke, S.; Craig, N.; Fisher, L.E.; et al. *The State of Coral Reef Ecosystems of Southeast Florida*; Nova Southeastern University: Davie, FL, USA, 2008.
68. Duke, N.; Ball, M.; Ellison, J. Factors influencing biodiversity and distributional gradients in mangroves. *Glob. Ecol. Biogeogr. Lett.* **1998**, *7*, 27–47. [CrossRef]

69. Quisthoudt, K.; Schmitz, N.; Randin, C.F.; Dahdouh-Guebas, F.; Robert, E.M.; Koedam, N. Temperature variation among mangrove latitudinal range limits worldwide. *Trees* **2012**, *26*, 1919–1931. [CrossRef]

70. Wilkinson, C.R. Global change and coral reefs: Impacts on reefs, economies and human cultures. *Glob. Change Biol.* **1996**, *2*, 547–558. [CrossRef]

71. Birkeland, C. *Life and Death of Coral Reefs*; Springer Science & Business Media: Berlin/Heidelberg, Germany, 1997.

72. Chen, P.Y.; Chen, C.C.; Chu, L.; McCarl, B. Evaluating the economic damage of climate change on global coral reefs. *Glob. Environ. Change* **2015**, *30*, 12–20. [CrossRef]

73. Pearce, A.; Jackson, G.; Moore, J.; Feng, M.; Gaughan, D.J. *The "Marine Heat Wave" off Western Australia during the Summer of 2010/11*; Report Fisheries Research Report No. 221; Government of Western Australia Department of Fisheries: Perth, Australia, 2011.

74. Holbrook, N.J.; Sen Gupta, A.; Oliver, E.C.; Hobday, A.J.; Benthuysen, J.A.; Scannell, H.A.; Smale, D.A.; Wernberg, T. Keeping pace with marine heatwaves. *Nat. Rev. Earth Environ.* **2020**, *1*, 482–493. [CrossRef]

75. Sheppard, C.; Dixon, D.J.; Gourlay, M.; Sheppard, A.; Payet, R. Coral mortality increases wave energy reaching shores protected by reef flats: Examples from the Seychelles. *Estuar. Coast. Shelf Sci.* **2005**, *64*, 223–234. [CrossRef]

76. Pennings, S.C.; Glazner, R.M.; Hughes, Z.J.; Kominoski, J.S.; Armitage, A.R. Effects of mangrove cover on coastal erosion during a hurricane in Texas, USA. *Ecology* **2021**, *102*, e03309. [CrossRef]

77. Liu, H.; Zhang, K.; Li, Y.; Xie, L. Numerical study of the sensitivity of mangroves in reducing storm surge and flooding to hurricane characteristics in southern Florida. *Cont. Shelf Res.* **2013**, *64*, 51–65. [CrossRef]

78. Del Valle, A.; Eriksson, M.; Ishizawa, O.A.; Miranda, J.J. Mangroves protect coastal economic activity from hurricanes. *Proc. Natl. Acad. Sci. USA* **2020**, *117*, 265–270. [CrossRef]

79. Raju, R.D.; Arockiasamy, M. Coastal Protection Using Integration of Mangroves with Floating Barges: An Innovative Concept. *J. Mar. Sci. Eng.* **2022**, *10*, 612. [CrossRef]

80. Ferrario, F.; Beck, M.W.; Storlazzi, C.D.; Micheli, F.; Shepard, C.C.; Airoldi, L. The effectiveness of coral reefs for coastal hazard risk reduction and adaptation. *Nat. Commun.* **2014**, *5*, 3794. [CrossRef]

81. Harney, J.N.; Grossman, E.E.; Richmond, B.M.; Fletcher Iii, C.H. Age and composition of carbonate shoreface sediments, Kailua Bay, Oahu, Hawaii. *Coral Reefs* **2000**, *19*, 141–154. [CrossRef]

82. IPCC. Managing the Risks of Extreme Events and Disasters to Advance Climate Change Adaptation. 2012; 582p. Available online: http://ipcc-wg2.gov/SREX/ (accessed on 10 October 2022).